Research Square

Preprints are preliminary reports that have not undergone peer review.
They should not be considered conclusive, used to inform clinical practice,
or referenced by the media as validated information.

Seismic Fragility Functions of Parameterized RC Curved Bridges Considering Stochastic Flood-induced Scouring Effect

Wenpeng WU

wuwenpeng@xtu.edu.cn

Xiangtan University

Jiacheng Li

Xiangtan University

Xin Ye

Xiangtan University

Jiqiu Zhou

Xiangtan University

Jiaqin Hou

PowerChina Zhongnan Engineering Co. Ltd

Research Article

Keywords: Bridge, Earthquake, Flood, Random Scour, Curved Bridge, Fragility

Posted Date: September 16th, 2026

DOI: https://doi.org/10.21203/rs.3.rs-10719516/v1

License: This work is licensed under a Creative Commons Attribution 4.0 International License.
Read Full License

Additional Declarations: No competing interests reported.

Seismic Fragility Functions of Parameterized RC Curved Bridges Considering Stochastic Flood-induced Scouring Effect

Wenpeng Wu[1*], Jiacheng Li[1], Xin Ye[1,2*], Jiqiu Zhou[1], Jiaqin Hou[3]

Abstract

Flood-induced scouring can significantly affect the dynamic response and seismic performance of irregular curved bridges. Most previous research simplified the scouring effects by assuming that the riverbed line reaches the maximum possible scour depth. However, due to the uncertainty of extreme flood events, the corresponding scour depth around the foundations of curved bridges exhibits considerable randomness. It is essential to quantify the impact of scour uncertainty on the seismic evaluation of such bridges. In addition, both the seismic input angle of ground motions and the curvature radius of the curved girder can have a significant impact on the evaluation process. Consequently, this study put forward an analysis framework based on machine learning (ML) method. In this framework, the stochastic scour depth is jointly taken into account with 36 other random variables, including the curvature radius of curved girder and 140 sets of ground motions with different incidence angles, so as to develop parameterized seismic fragility models for curved bridge. A parameterized finite element model of reinforced concrete (RC) curved bridges is constructed within the OpenSees software, taking into consideration uncertainties stemming from structural design, flood-induced scour, and seismic excitation. A database composed of 1400 sets of input parameters and the corresponding engineering demand parameters (*EDPs*) is generated via Latin Hypercube Sampling (LHS) and nonlinear time history analyses that reuse 140 sets of ground motions. Based on the aforementioned data, a multidimensional probabilistic seismic demand model (MPSDM) founded on support vector regression (SVR) is established to estimate the failure probabilities of bridge's pier, bearing, pile foundation, and abutment, as well as to develop fragility models taking into account random scour, seismic incidence angles, and the curvature of curved girder. The predictive accuracy of the proposed model is validated through comparisons of R^2 and *RMSE* with those of the traditional linear PSDM, showing that the proposed SVR-based MPSDM provides a more accurate representation of the nonlinear response relationships for all selected engineering demand parameters. Moreover, once trained, the MPSDM allows direct fragility estimation for arbitrary combinations of scour depth, curvature radius, seismic incidence angle, and ground-motion intensity, without repeating nonlinear time-history analyses for each scenario. The results indicate that deeper scour, a smaller curvature radius, and unfavorable input directions significantly increase the component damage probability and shift critical damage from some pier sections toward pile foundations and displacement-controlled boundary components. The proposed framework provides a practical basis for multi-parameter fragility assessment for curved bridges in flood-prone regions.

*Xing Ye (corresponding author)

[1] College of Civil Engineering, Xiangtan University,Xiangtan, China

[2] School of Civil Engineering, Central South University, Changsha, China

[3] PowerChina Zhongnan Engineering Co. Ltd, Changsha, , China

Keywords: Bridge; Earthquake; Flood; Random Scour; Curved Bridge; Fragility

1. Introduction

Bridges are critical components of highway transportation systems, and their service safety is directly related to the continuous operation of transportation networks and post-disaster emergency response. Among various natural hazards, earthquakes and flood-induced scour are two major factors affecting bridge safety. The former may cause component damage or even structural failure, whereas the latter can weaken foundation restraint and amplify the risk of seismic damage. Compared with traditional regular bridges, curved bridges have been widely used in recent years because they can better accommodate complex roadway alignments with their unique geometric structures. However, their geometric irregularity leads to more complicated structural behavior and dynamic response under unpredictable external extreme loads.

On the one hand, post-earthquake investigations have revealed that curved bridges generally endure more severe damage compared to straight bridges. Under seismic excitation, the main girder might experience spatial motion, which can generate complex force demands in piers and bearings and subsequently lead to seismic damage such as bearing unseating and girder collapse **(Yang and Ma 2018)**. Recent large-scale hybrid tests have further verified that small-radius curved bridges may display complex spatial failure modes under earthquake loading, and their observed damage patterns are generally in line with post-earthquake field observations **(Tian et al. 2024)**. Therefore, significant efforts have been dedicated to exploring the seismic response and fragility of curved bridges. **Jiao et al. (2018)** reported that a smaller curvature radius results in more prominent differences in transverse internal forces and displacements among bridge piers. **Tondini and Stojadinovic (2012)** established a probabilistic seismic demand model for curved reinforced concrete bridges and identified the radius of curvature as a crucial parameter influencing seismic demand. **Jeon et al. (2016)** further investigated the effects of horizontal curvature, abutment skew angle, and pier height on the seismic demand and fragility of multi - frame curved concrete box-girder bridges, indicating that geometric irregularity can substantially change the seismic response of the structure. **Uenaga et al. (2023)** further demonstrated that deck radius, pier - height irregularity, and incident angle jointly affect the fragility and resilience of curved reinforced concrete bridges under both short - and long - period ground motions. **Abbasi et al. (2016)** analyzed multi - frame curved concrete box multi-supports and probed their seismic response under different curvature radii and pier heights. **Feng et al. (2018)** showed that the angle of seismic incidence has a significant impact on the IM based components and the overall bridge system. From the perspective of more realistic seismic input. **Song et al. (2024)** demonstrated that spatially varying multi-support ground motions can significantly

affect the fragility and fragility estimates of multi-span irregular curved bridges. **Rashid and Nishio (2025)** further developed optimal intensity-measure-based seismic fragility surfaces for curved bridges and emphasized their sensitivity to seismic excitation direction. **Tehrani and Heydarpour (2025)** also showed that varying earthquake incidence angles can notably influence the seismic response prediction of horizontally curved reinforced concrete bridges under bidirectional ground motions. **Serdar and Folić (2018)** pointed out that, in comparison to conventional straight bridges, curved bridges involve greater complexity in seismic demand modeling and fragility assessment, and that the selection of an optimal probabilistic seismic demand model (PSDM) merits special attention. Overall, previous studies have offered substantial understanding of the effects of curvature radius, pier height, and seismic incidence angle on the seismic response of curved bridges.

On the other hand, flood-induced scour is another important external factor affecting the seismic performance of bridges. Existing studies have shown that scour can reduce the foundation embedment depth and lateral restraint, thereby altering the dynamic characteristics of bridges and increasing their fragility under seismic loading **(Li G 2022)**. **Ateş and Avşar (2023)** investigated the influence of scour depth on the natural vibration period and superstructure displacement demand of skewed highway girder bridges. **Ateş and Avşar (2024)** has also shown that both uniform and non-uniform scour can markedly affect the seismic performance of skewed bridges, with the response being further influenced by the angle of ground-motion incidence. **Wang et al. (2014)** found that increasing the scour depth leads to a longer vibration period, and that different bridge types exhibit different levels of sensitivity to the scour depth. **Ganesh Prasad and Banerjee (2013)** and **Annad et al. (2023)** showed that an increase in the scour depth significantly raises the seismic fragility of reinforced concrete bridges. **Li et al. (2025)** and **Pinto et al. (2024)** further indicated that uncertainty in the scour condition can significantly influence the seismic fragility estimates of simply supported reinforced concrete bridges. **Wu et al. (2024)** further pointed out that, as the degree of flood scour increases, the seismic fragility of the bridge system continues to increase, while the damage sequence and damage progression of different components also change markedly. **Hung and Yau (2017)** and **Guo et al. (2016)** demonstrated, from the perspectives of soil - structure - water interaction and multi - parameter uncertainty, respectively, that increasing the scour depth and seismic intensity can significantly aggravate bridge damage. From a broader multi - hazard perspective, **Biazar et al. (2024)** proposed a fragility modeling framework for bridges with shallow foundations subjected to combined earthquake, scour, and vehicular loading, highlighting the importance of jointly considering interacting hazards. **Karriqi et al. (2024)** further proposed an integrated bridge assessment framework under earthquake and flood-induced scour, and generated fragility curves for both component - level and system - level performance under different multi - hazard scenarios. **Ge et al. (2023)**

extended bridge fragility assessment to a time- dependent multi - hazard setting involving deterioration, climate change, earthquakes, and flood-induced scour. **Medina Yauri et al. (2026)** proposed an integrated resilience assessment framework for riverine bridges, enabling a more comprehensive evaluation in flood-dominated yet multi-hazard environments. At the network level, **Ansari et al. (2024)** demonstrated that bridge failures under combined earthquake and flood scenarios may trigger cascading effects, leading to substantial reductions in overall system performance. At the broader infrastructure level, **Nirandjan et al. (2024)** reviews and resilience studies have also highlighted the growing need for multi - hazard fragility and decision - support frameworks for critical infrastructure systems. These studies indicate that scour not only modifies the dynamic characteristics of bridges but also further amplifies seismic damage by weakening foundation stability.

Although previous studies have separately revealed the seismic response characteristics of curved bridges and the adverse effects of flood-induced scour on bridge safety and dynamic performance, research on the seismic fragility of curved bridges under combined scour-earthquake effects remains limited. In particular, many previous studies simply simplified the scour effects by assuming that the ground line reaches the maximum possible scour depth. Due to the uncertainty of extreme flood events, the scour depth around the foundations of curved bridges exhibits considerable randomness. It is therefore essential to quantify the impact of scour-depth uncertainty on the seismic performance of such bridges. In addition, when multiple sources of uncertainty, such as scour depth, ground-motion intensity, seismic incidence angle, and curvature radius of the curved girder, are considered simultaneously, efficient and reliable assessment methods are still lacking. However, traditional analytical methods, such as the linear and explicit probabilistic seismic demand models (PSDM), have faced significant computational challenges when dealing with the numerous uncertainty sources mentioned above, making it difficult to analyze the interrelationships between different influencing factors and their sensitivities. In recent years, machine learning technologies **(Rezaei et al. 2022; Parisi et al. 2025)** have provided an effective solution to overcome these issues. By employing machine-learning approaches, researchers can not only enhance analytical accuracy while substantially reducing the workload of structural finite element calculations but also demonstrate strong compatibility with sensitivity analysis processes **(Rezaei et al. 2023; Ning et al. 2024; Saida et al. 2024).**

Despite these advancements, several important issues remain unresolved. Firstly, flood-induced scour is still commonly idealized as a deterministic maximum scour depth, which neglects its inherent uncertainty under extreme hydraulic conditions. Secondly, the combined influences of scour depth, curvature radius, seismic incidence angle, and ground-motion intensity on the fragility of curved bridges have not yet been systematically quantified within a unified probabilistic framework. Third, conventional single-parameter fragility

models are insufficient to capture the nonlinear interaction effects among multiple governing variables. Consequently, this study focuses on evaluating: (1) the influence of stochastic scour depth on the seismic fragility of curved RC bridges; (2) the effects of curvature radius and seismic incidence angle on component-level fragility under scour conditions; and (3) the predictive capability of the proposed machine-learning model in comparison with conventional linear fragility approaches. Accordingly, the following hypotheses are examined: (H1) Increasing scour depth significantly alters the seismic fragility distribution among bridge components, leading to increased fragility in foundations and displacement-controlled boundary components.; (H2) Curvature radius and seismic incidence angle produce measurable changes in component-level fragility; (H3) The proposed machine-learning-based multidimensional demand model provides higher predictive accuracy than conventional linear fragility models. The main contribution of this work is the development of a multidimensional fragility assessment framework that simultaneously incorporates scour uncertainty, seismic intensity, seismic incidence angle, and bridge curvature. The findings are expected to provide useful guidance for seismic design, resilience assessment, and scour mitigation strategies for curved bridges located in flood-prone regions.

In general, this study proposes a machine-learning-based framework for developing seismic fragility models of RC curved bridges subjected to stochastic flood-induced scour and earthquake excitation. A series of representative horizontally curved reinforced concrete bridges with varying geometric characteristics are selected as case-study structures. Parametric finite-element models are established, and a database of structural responses is generated through Latin hypercube sampling and nonlinear time-history analyses. Based on these data, support vector regression is employed to construct a multidimensional probabilistic seismic demand model capable of accounting for multiple uncertain variables simultaneously.

2. Fragility Analysis of Curved Bridges Based on SVR Machine Learning

2.1 Machine Learning-Based fragility Analysis Framework

Over the past decades, extensive studies and practical applications have led to the development and refinement of a series of classical methods for seismic fragility analysis of bridges **(Li et al. 2024)**. These methods include, for example, the cloud method, the IDA-based scaling method, the demand-to-capacity ratio-based logarithmic regression method, and fragility analysis based on maximum likelihood estimation. However, most of these approaches remain essentially parametric. In recent years, increasing attention has been paid to non-parametric fragility analysis methods, which do not require prior assumptions regarding the shape of seismic fragility curves and therefore can improve the accuracy of fragility assessment while reducing model bias **(Li**

et al. 2024). Non-parametric seismic fragility analysis methods mainly include conditional Monte Carlo simulation, kernel density estimation, and machine-learning-based approaches. Among these, machine learning can effectively quantify the high-dimensional nonlinear relationships between input variables and seismic response, thereby enabling the construction of a multidimensional probabilistic seismic demand model (MPSDM). Compared with traditional methods, this approach can improve both the prediction accuracy of structural seismic response and the computational efficiency of fragility assessment **(Lu et al. 2022; Zheng et al. 2023; Zhong et al. 2025)**.

As shown in **Fig. 1**, the machine-learning-based parametric multidimensional seismic fragility analysis framework mainly consists of two major parts. The first part involves parametric bridge modeling, dynamic analysis, and machine learning, aiming to establish a ML-based multidimensional probabilistic seismic demand model (MPSDM). At this stage, multiple sources of uncertainty associated with the bridge structure itself, flood hazards, and seismic hazards can be considered simultaneously. For example, in the present study, the curvature radius of the curved girders, random scour depth, and seismic input angle of the bridge are all incorporated into the bridge ground motion sample database. After a large number of nonlinear time-history analyses are conducted, the resulting input–output relationships are mapped to the machine learning model, the proposed MPSDM shown in **Fig. 1**.The second part is the multidimensional seismic fragility analysis of bridge structures. As illustrated in **Fig. 1**, this part contains both inner and outer iterative loops. Through the inner loop, seismic fragility curves for a target bridge structure under different damage states can be established. Here, the target bridge structure may refer to either a specific bridge or a class of bridges sharing the same structural characteristics. The outer loop is used to further account for the effects of hazard - related or design-related parameters other than ground - motion intensity. For instance, when the variable Y represents the scour depth Hs of the bridge substructure, a joint fragility surface with respect to seismic intensity and scour depth can be constructed to investigate the influence of Hs on bridge seismic fragility. When Y represents the seismic input direction θ, a joint fragility surface with respect to ground-motion intensity and input direction can be developed to examine the influence of θ on bridge seismic fragility.

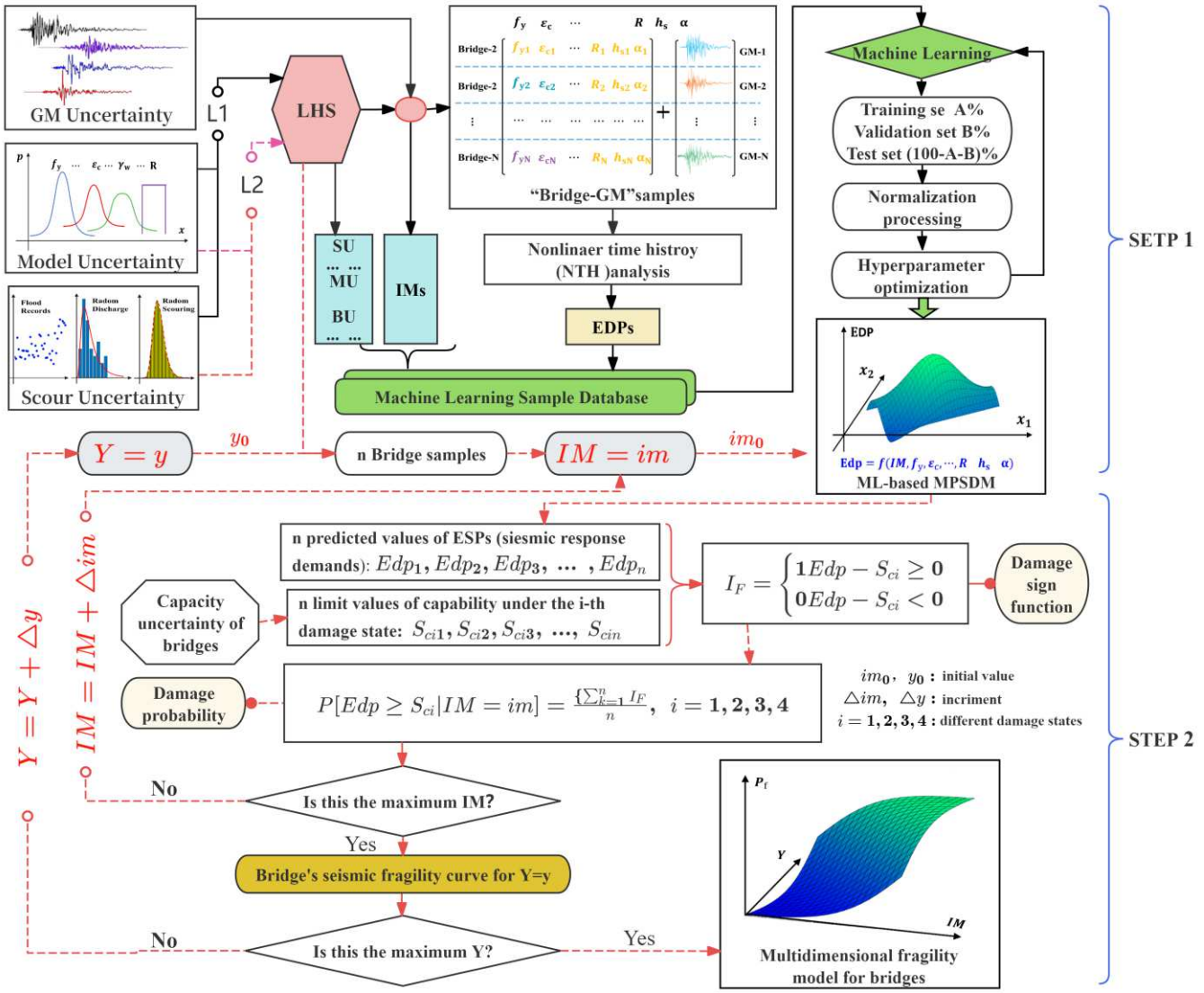


Fig.1 Parametric multidimensional seismic fragility analysis flowchart based on machine learning

Currently, the ML methods can generally be categorized into three main types: supervised learning, unsupervised learning, and semi-supervised learning. As shown in **Fig. 1**, an appropriate ML method can be selected by comprehensively considering the scale of the input data-set, computational accuracy, and analysis efficiency. It is worth noting that in recent years, extensive comparative research has been conducted on the performance of different ML algorithms in fragility and seismic demand prediction. For example, **Nguyen et al. (2023)** compared Random Forest, Gradient Boosting, ANN, and XGBoost for the seismic fragility assessment of steel moment frames and indicated that the superiority of the model depends on the characteristics of the data-set. **Ding et al. (2023)** evaluated SVM, ANN, DT, RF, XGBoost within a probabilistic fragility framework and reported that different algorithms have their own advantages in different evaluation dimensions. **Jabari Salmi et al. (2024)** further compared Decision Tree, Random Forest, Logistic Regression, SVM, Gradient Boosting, and XGBoost for estimating fragility parameters, once again demonstrating that the predictive performance is problem - dependent. In bridge engineering, **Soleimani (2022)** also verified the effectiveness of multiple ML approaches for the probabilistic seismic analysis of bridges.

Although various methods, such as artificial neural networks, logistic regression, support vector regression (SVR), decision trees, and random forests, have been applied in previous studies on bridge seismic fragility analysis**(Kiani et al. 2019; Ruchun et al. 2023; Zheng et al. 2023)**, the main objective of the present study is not to identify the optimal ML algorithm, but to establish a multidimensional probabilistic seismic demand framework for RC curved bridges that explicitly captures the coupled effects of stochastic scour depth, seismic intensity, curvature radius, and incidence angle on seismic fragility . Therefore, the present study uses the SVR algorithm as an example to conduct machine learning on the relevant data, due to its well-documented robustness and strong generalization ability for medium - sized datasets and high - dimensional nonlinear regression problems, which are consistent with the characteristics of the current bridge fragility database.

2.2 Principles of SVR and the Optimal Decision Model

Support Vector Machine (SVM) is a supervised learning algorithm applicable to both classification and regression tasks. When applied to classification problems, it is referred to as Support Vector Classification (SVC), and when handling regression problems, it is called Support Vector Regression (SVR)**(Ruchun et al. 2023)**. The core of SVC is to find the optimal classification hyperplane to maximize the margin between samples. As shown in **Fig.2**, in a two-dimensional space, data separation is achieved by constructing the function $y^{(t)} = w^T \phi(x^t) + b$, thereby forming the optimal model. SVR, on the other hand, constructs a regression model to make sample points approach it, ensuring smoothness. It seeks the optimal fitting model $y^{(t)} = w^T \phi(x^t) + b$ in a two - dimensional space. This study employs the SVR algorithm. Its model is determined by a small number of support vectors, and its performance relies on these. Computational efficiency is determined by the number of support vectors, making SVR efficient and having strong generalization capabilities when dealing with high-dimensional nonlinear problems, and stable in prediction even with small samples.

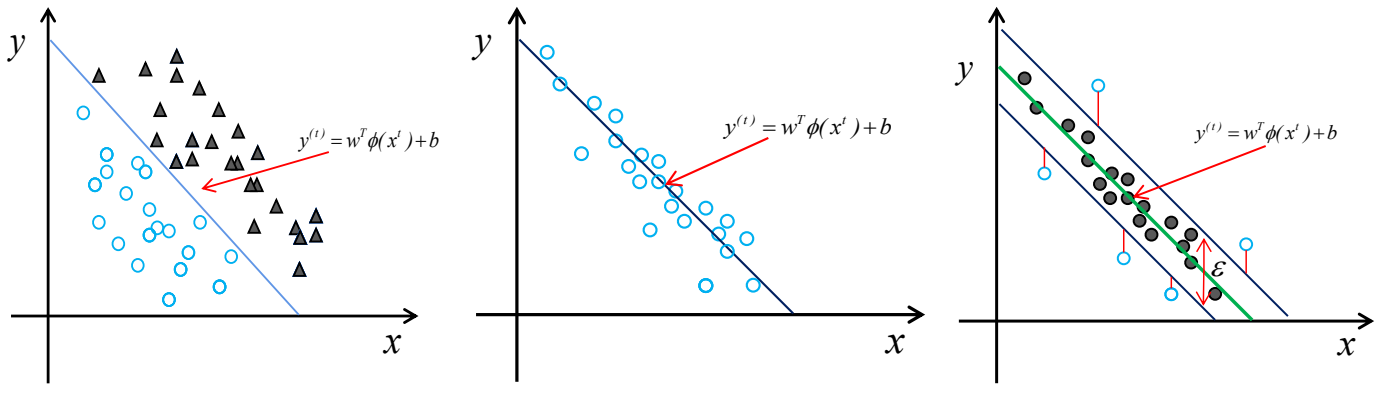


Fig.2 Basic principle of SVM method: (a) classification; (b) regression; (c) loss function.

SVR uses a loss function to measure prediction error, typically employing an insensitive loss function as shown in Equation (1). When the error is less than ε, the loss is 0, thus ignoring minor errors to reduce sensitivity. A penalty is applied only when the error exceeds the ε threshold.

$$\text{error}=\begin{cases} 0 & |\ y^{(t)}-(w^T\phi(x^t)+b)|\le\varepsilon \\ y^{(t)}-(w^T\phi(x^t)+b)-\varepsilon & |\ y^{(t)}-(w^T\phi(x^t)+b)|>\varepsilon \end{cases} \tag{1}$$

where ε represents the error threshold or constant. As shown in **Fig. 2**, the loss for data points inside the two blue bands is zero, while the loss for points outside is the red vertical length from the point to the blue boundary.

Furthermore, SVR requires the introduction of a kernel function for nonlinear regression to map the input to a high - dimensional space for linear regression. The choice of the kernel function influences the algorithm's performance. The penalty factor *C* is also crucial: an excessively large *C* leads to over fitting (good performance on the training set but poor generalization on the test set), while an excessively small *C* leads to under fitting, resulting in high errors and an inability to perform correct regression. Therefore, a reasonable selection of the penalty factor *C* is essential for the performance of the SVR model. An appropriate *C* value ensures the model neither overfits nor underfits, thereby maintaining good generalization ability while improving the accuracy of regression predictions. The optimal value for the penalty factor *C* is typically determined and adjusted on the training set using cross - validation. Based on the above, the objective function and constraints for the regression problem are:

$$\min\frac{1}{2}\|\ w\|^2 \tag{2}$$

$$\text{s.}t.|\ y^{(i)}-(w^T\phi(x^t)+b)|\le\varepsilon,\quad t=1,.....,n \tag{3}$$

At this point, to minimize the influence of noise points as much as possible and allow for a greater margin of error, slack variables ξ_t^v and ξ_t^α are further introduced. Therefore, the objective optimization problem is transformed into:

$$\min\frac{1}{2}\|\ w\|^2+C\sum_{t=1}^{n}(\xi_t^v+\xi_t^\alpha) \tag{4}$$

$$\text{s.t.}\begin{cases} y^{(t)}-\left(w^T\phi(x^{(t)})+b\right)\le\grave{o}+\xi_t^v \\ \left(w^T\phi(x^{(t)})+b\right)-y^{(t)}\le\grave{o}+\xi_t^\alpha \\ \xi_t^v\ge0,\quad \xi_t^\alpha\ge0,\quad t=1,...,n \end{cases} \tag{5}$$

Based on the above, the Lagrange function is constructed, and the equation is as follows:

$$L(w,b,\xi^{v},\xi^{\alpha},\alpha^{v},\alpha^{\alpha},\mu^{v},\mu^{\alpha})=\frac{1}{2}\|w\|^{2}+C\sum_{t=1}^{n}(\xi_{t}^{v}+\xi_{t}^{\alpha})+\sum_{t=1}^{n}\alpha_{t}^{v}\left[y^{(t)}-\langle w,\phi(x^{t})\rangle-b-\grave{o}-\xi_{t}^{v}\right]$$
$$+\sum_{t=1}^{n}\alpha_{t}^{\alpha}\left[\langle w,\phi(x^{t})\rangle+b-y^{(t)}-\grave{o}-\xi_{t}^{\alpha}\right]-\sum_{t=1}^{n}\mu_{t}^{v}\xi_{t}^{v}-\sum_{t=1}^{n}\mu_{t}^{\alpha}\xi_{t}^{\alpha}, \tag{241}$$

$$\xi_{t}^{v},\xi_{t}^{\alpha},\alpha_{t}^{v},\alpha_{t}^{\alpha},\mu_{t}^{v},\mu_{t}^{\alpha}\geq 0,\quad t=1,\ldots,n \tag{6}$$ 242

By taking partial derivatives of the parameters $w,b,\xi_{t}^{v},\xi_{t}^{\alpha}$ in the Lagrange function with respect to each unknown variable and setting them equal to 0, the following equations are obtained through the solution process: 243 244

$$w=\sum_{t=1}^{n}\left(\alpha_{t}^{v}-\alpha_{t}^{\alpha}\right)\phi(x^{(t)}) \tag{7}$$ 245

$$\sum_{t=1}^{n}(\alpha_{t}^{v}-\alpha_{t}^{\alpha})=0 \tag{8}$$ 246

$$0\leq\alpha_{t}^{v}\leq C,\ \ t=1,\ldots,n \tag{9}$$ 247

$$0\leq\alpha_{t}^{\alpha}\leq C,\ \ t=1,\ldots,n \tag{10}$$ 248

Substituting the partial - derivative results from (7) to (10) into the Lagrange function in (6), the dual form of the optimization problem is obtained as: 249 250

$$\max\sum_{t=1}^{n}y^{(t)}(\alpha_{t}^{v}-\alpha_{t}^{\alpha})-\grave{o}\sum_{t=1}^{n}(\alpha_{t}^{v}+\alpha_{t}^{\alpha})-\frac{1}{2}\sum_{i=1}^{n}\sum_{j=1}^{n}(\alpha_{i}^{v}-\alpha_{i}^{\alpha})(\alpha_{j}^{v}-\alpha_{j}^{\alpha})\langle\phi(x^{(i)}),\phi(x^{(j)})\rangle$$
$$\text{s.t.}\begin{cases}\sum_{t=1}^{n}(\alpha_{t}^{v}-\alpha_{t}^{\alpha})=0,0\leq\alpha_{t}^{v},\\ \alpha_{t}^{\alpha}\leq C,\quad t=1,\ldots,n\end{cases} \tag{11}$$ 251

Similarly, for nonlinear problems, replacing the inner product operation in the above equation with the kernel function $K\left(x^{(t)},x\right)$ yields the learning model of the support vector machine as: 252 253

$$f(x)=\sum_{t=1}^{n}\left(\alpha_{t}^{v}-\alpha_{t}^{\alpha}\right)K\left(x^{(t)},x\right)+b \tag{12}$$ 254

3. Bridge Modelling and Uncertainty Sources 255

3.1 Case-Study Bridge 256

The case-study bridge is founded upon a prototype of a six-span curved girder bridge spanning a river in western China. The total length of the bridge is 150 meters, (with a span arrangement of 6 × 25 meters, and the width of the deck is 11.8 m. The superstructure is composed of seven C50 concrete girders with a height of 1.2 m. The center-line of the bridge follows a circular curve with a radius of R. The bent cap has a rectangular cross-section measuring 1.5 m × 1.7 m. The piers are of a double-column C40 concrete frame structure, where each column has a diameter of 1.6 m and is fabricated from C40 concrete. The bottom of the pier columns is connected by a transverse tie beam, and the height of the piers is 15 meters. The pier foundation adopts RC bored cast-in-place piles with a diameter of 1.8 m and a length of 19.6 m, which are constructed 257 258 259 260 261 262 263 264

using C30 concrete. The width of the expansion joint between the abutment and the girder end is 11 cm. Both the pier tops and abutments utilize laminated rubber bearings. The overall layout is depicted in **Fig. 3.** Based on the design data of the case-study bridge, the backfill soil behind the abutment is artificial sandy fill. The soils at the abutment and pier locations, including the pile cap and pile foundation areas, are predominantly composed of silty sand and sandy clay. The bearing stratum beneath the pile tips is completely weathered limestone.

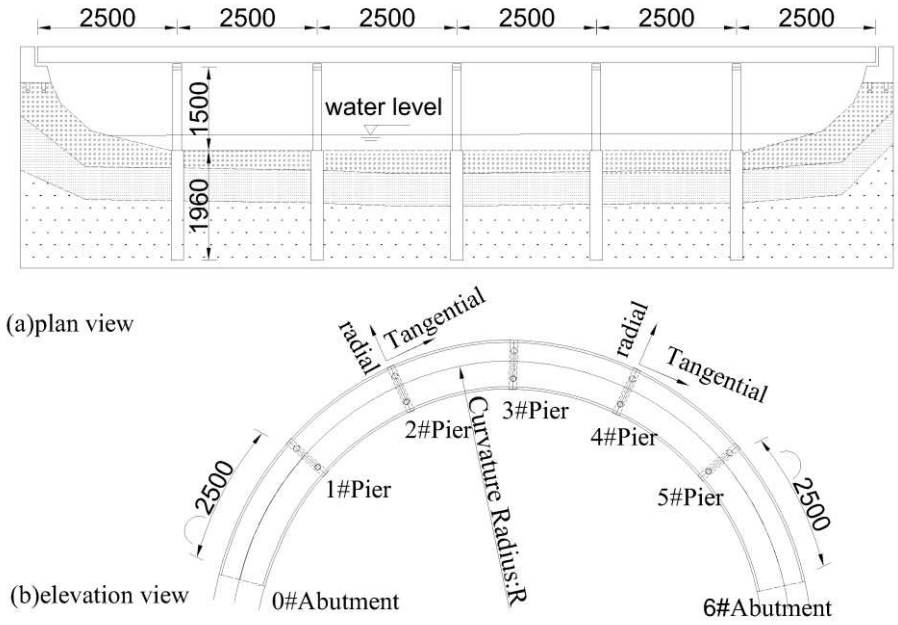


Fig.3 Schematic diagram of a bridge (unit: cm)

3.2 Parameterized Finite Element Model

This research established a nonlinear finite element dynamic analysis model for the aforementioned curved bridge on the OpenSees platform, as shown in **Fig. 4**. The superstructure components, namely the main girders, bent caps, and tie beams, were simulated by means of elastic beam elements. The piers and pile foundations were modeled with nonlinear fiber elements. The constitutive behaviors of concrete and reinforcing steel were respectively characterized by the Concrete04 and Steel02 material models to consider their material non-linearity. To more realistically simulate the response characteristics of the bridge under seismic excitation, the model also incorporated the nonlinear effects of key components such as abutments, bearings, expansion joints, and shear keys, as well as the pile - soil interaction. These characteristics were simulated using Zero - Length elements. The specific modeling methodology can be referred to in the relevant literature**(Li et al. 2020; Li et al. 2024; Wu et al. 2025).**

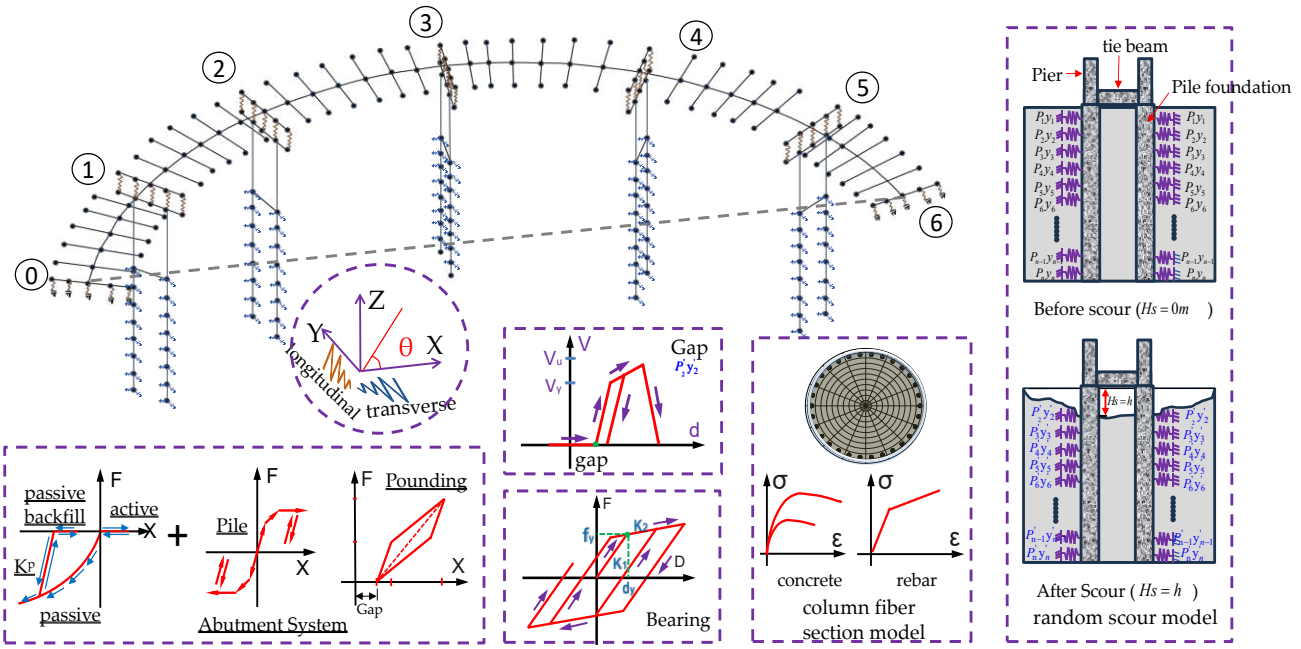


Fig.4 OpenSees Finite element model of case-study bridge

To further validate the rationality of the prototype model, the global dynamic characteristics of the bridge were investigated under varying scour depths. **Table 1** presents the first three natural periods of the bridge for *Hs* = 0, 5, 10, and 15 m. It can be discerned that all three natural periods increase gradually as the scour depth increases. In comparison with the intact state, the first three periods increase by 4.9%, 5.3%, and 27.4% at *Hs* = 5 m, by 14.2%, 15.6%, and 34.6% at *Hs* = 10 m, and by 36.9%, 39.2%, and 50.1% at *Hs* = 15 m, respectively. This tendency is in line with the anticipated reduction in foundation restraint and the corresponding enhancement in global structural flexibility induced by scour. Therefore, the variation of modal properties corroborates the rationality of the scour - updated numerical model employed in the current study. Additionally, the constitutive assumptions for representative nonlinear components were verified against previously validated studies of analogous bridge systems.

Table 1. Modal properties of the bridge under different scour depths

Hs(m)	*T1*	Increment	*T2*	Increment	*T3*	Increment
0	0.670	0%	0.584	0%	0.387	0%
5	0.703	4.90% ↑	0.615	5.30% ↑	0.493	27.4% ↑
10	0.765	14.2% ↑	0.675	15.6% ↑	0.521	34.6% ↑
15	0.917	36.9% ↑	0.813	39.2% ↑	0.581	50.1% ↑

It is particularly noteworthy that, given the differences in tangential and radial azimuth angles at various piers and abutments of the case-study bridge (refer to **Fig.3**), the local coordinate system of the aforementioned Zero - Length elements in the model must be defined as a function of parameters such as the curvature radius

R and span length. Moreover, since the subsequent research also takes into account the random flood - induced scouring effect, the parameters of the PySimple1 model for the pile - soil Zero - Length elements will vary with the scour depth**(Wu et al. 2025)**. As the scour depth increases, the surrounding soil layers around the foundations are gradually eroded, leading to a significant reduction in lateral stiffness and load - carrying capacity. Therefore, in this study, the lateral p - y spring elements within the scour depth (*Hs*) were removed**(Tubaldi et al. 2018; Scozzese et al. 2023)** to simulate the effects of flood - induced scour in the updated finite element (FE) models. Additionally, the lateral stiffness of the remaining p–y springs below the scour line was adjusted accordingly to account for the loss of upper soil support. **Fig. 4** depicts the scoured pile - soil - interaction model with the updated *p-y* springs.

3.3 Input Parameters and Uncertainties

In the construction of the ML sample database for this research, a total of 39 random parameters were chosen as input variables. **Table 2** presents the mean (μ), standard deviation (σ), and corresponding probability distribution types for all input variables. Among them, *X1* to *X35* signify uncertainty parameters associated with structural modeling, encompassing those related to structural unit weight, sub - structure (pier, pile) dimensions and materials, as well as diverse boundary condition parameters. *X36* represents the random flood - induced scour depth, *X37* denotes the curvature radius of the girder centerline, and *X38* to *X39* are parameters related to ground motion. This study utilizes Latin Hypercube Sampling (LHS) to sample the input variables from the parameter ranges specified in **Table 2**, thus generating bridge model - ground motion analysis samples. Simultaneously, the sampled values of these uncertain parameters will act as the numerical inputs for the ML model.

Table 2. Uncertainty parameters of bridges and their probability distributions

Input	Symbol (unit)	Distribution	Input	Symbol (unit)	Distribution
X1	λ_w	$N(\mu=1.06,\mathrm{COV}=10\%)$	*X21*	$\varepsilon_{\mathrm{ccu_pile}}$	$LN(\mu=0.015,\mathrm{COV}=30\%)$
X2	D(m)	$N(\mu=1.6,\mathrm{COV}=5\%)$	*X22*	E_s(MPa)	$LN(\mu=2\mathrm{E}5,\mathrm{COV}=3\%)$
X3	c(m)	$N(\mu=0.05,\mathrm{COV}=10\%)$	*X23*	f_y(MPa)	$LN(\mu=378,\mathrm{COV}=7\%)$
X4	$D_{_pile}$(m)	$N(\mu=1.8,\mathrm{COV}=5\%)$	*X24*	B	$LN(\mu=0.0012,\mathrm{COV}=20\%)$
X5	$c_{_pile}$(m)	$N(\mu=0.08,\mathrm{COV}=5\%)$	*X25*	μ_{PTEB}	U(0.2,0.3)
X6	d(mm)	$N(\mu=32,\mathrm{COV}=3.5\%)$	*X26*	G_{PTEB}(MPa)	$N(\mu=1.2,\mathrm{COV}=14\%)$
X7	ξ	$N(\mu=0.05,\mathrm{COV}=15\%)$	*X27*	K_{P_LRB}(kN/m)	$N(\mu=1500,\mathrm{COV}=14\%)$

X8	$E_{\text{c_pier}}$(MPa)	$LN(\mu = 3.25\text{E}4, \text{COV}=14\%)$	*X28*	P_{ult}(kN)	U(0.5*P*,1.5*P*)
X9	$f_{\text{c_pier}}$(MPa)	$LN(\mu = 32, \text{COV}=20\%)$	*X29*	$K_{Passive}$(kN/m)	U($0.5K_P$,$1.5K_P$)
X10	$\varepsilon_{\text{c_pier}}$	$LN(\mu = 0.002, \text{COV}=20\%)$	*X30*	K_{Active}(kN/m)	U($0.5K_A$,$1.5K_A$)
X11	$\varepsilon_{\text{cu_pier}}$	$LN(\mu = 0.006, \text{COV}=20\%)$	*X31*	Δ(m)	U(0.08,0.12)
X12	$f_{\text{cc_pier}}$(MPa)	$LN(\mu = 39, \text{COV}=20\%)$	*X32*	K_{eff}(kN/m)	$LN(\mu = 1.94\text{E}6, \text{COV}=14\%)$
X13	$\varepsilon_{\text{cc_pier}}$	$LN(\mu = 0.004, \text{COV}=20\%)$	*X33*	f_{yy}(MPa)	$LN(\mu = 378, \text{COV}=7\%)$
X14	$\varepsilon_{\text{ccu_pier}}$	$LN(\mu = 0.016, \text{COV}=20\%)$	*X34*	f_{uy}(MPa)	$LN(\mu = 520, \text{COV}=7\%)$
X15	$E_{\text{c_pile}}$(MPa)	$LN(\mu = 3\text{E}4, \text{COV}=14\%)$	*X35*	δ(m)	U(0.03,0.10)
X16	$f_{\text{c_pile}}$(MPa)	$LN(\mu = 24, \text{COV}=14\%)$	*X36*	H_s(m)	$LN(\mu = 7.2, \text{COV}=26\%)$
X17	$\varepsilon_{\text{c_pile}}$	$LN(\mu = 0.002, \text{COV}=20\%)$	*X37*	*R*(m)	U(50, 200)
X18	$\varepsilon_{\text{cu_pile}}$	$LN(\mu = 0.006, \text{COV}=20\%)$	*X38*	θ	U($0, 2\pi$)
X19	$f_{\text{cc__pile}}$(MPa)	$LN(\mu = 30, \text{COV}=21\%)$	*X39*	*PGV*	Discrete
X20	$\varepsilon_{\text{cc_pile}}$	$LN(\mu = 0.004, \text{COV}=20\%)$			

*N denotes normal distribution, LN denotes lognormal distribution, and U denotes uniform distribution. λ_w and ξ represent the structural unit weight coefficient and damping ratio, respectively. $D_{\text{_pier}}$ and $c_{\text{_pier}}$ represent the pier column diameter and concrete cover thickness. $D_{\text{_pile}}$ and $c_{\text{_pile}}$ represent the pile foundation diameter and concrete cover thickness. $E_{\text{c_pier}}$, $f_{\text{c_pier}}$, $\varepsilon_{\text{c_pier}}$, $\varepsilon_{\text{cu_pier}}$, $f_{\text{cc_pier}}$, $\varepsilon_{\text{cc_pier}}$ and $\varepsilon_{\text{ccu_pier}}$ represent the elastic modulus, unconfined compressive strength, unconfined peak compressive strain, unconfined ultimate compressive strain, confined compressive strength, confined peak compressive strain, and confined ultimate compressive strain of the C40 concrete for the pier columns, respectively. $E_{\text{c_pier}}$, $f_{\text{c_pier}}$, $\varepsilon_{\text{c_pier}}$, $\varepsilon_{\text{cu_pier}}$, $f_{\text{cc_pier}}$, $\varepsilon_{\text{cc_pier}}$ and $\varepsilon_{\text{ccu_pier}}$ represent the corresponding parameters for the C30 concrete of the pile foundations. d, E_s, f_y and B represent the reinforcing bar diameter, elastic modulus, yield strength, and strain hardening ratio, respectively. P_{ult}, K_{Passive} and K_{Active} represent the abutment passive ultimate capacity, passive tangent stiffness, and active effective stiffness, respectively. Δ and K_{eff} represent the expansion joint gap width and effective impact stiffness. f_{yy}, f_{uy} and δ represent the shear key (or restrainer) bar yield strength, ultimate strength, and shear key gap, respectively. H_s, R and θ denotes the flood-induced scour depth, horizontal curvature radius of the curved girder, respectively. PGV represent the peak ground velocity.

In the annotation at the end of Table 2, the designations and connotations of each input variable are enumerated. For parameters *X1-X35* in Table 2, their values and uncertainties were determined based on the actual conditions of the case-study bridge and with reference to existing literature**(Li et al. 2020; Hu et al. 2022; Wu et al. 2025)**. Regarding the random flood - induced scour depth *X36*, this research utilizes the

modified formula based on the CSU equation in HEC - 18 to compute the local scour depth at bridge piers**(Arneson et al. 2012)**:

$$y_{\mathrm{ps}} = 2.0\lambda_s y_{p0} K_{p1} K_{p2} K_{p3} \left(\frac{a}{y_{p0}}\right)^{0.65} \left(\frac{V_{p0}}{\sqrt{g \cdot y_{p0}}}\right)^{0.43} \quad (13)$$

where, y_{ps} , y_{p0} and V_{p0} respectively denote the local scour depth, water depth, and flow velocity at the pier location; a represents the effective width of the pier perpendicular to the flow direction. λ_s、K_{p1}、K_{p2}、K_{p3} are coefficients associated with the model, pier shape, flow attack angle, and flow conditions, respectively; g signifies the gravitational acceleration (9.8 m/s²). This research gathered 40 - year historical annual peak discharge data at the bridge site and conducted frequency analysis, as presented in Fig. 5(a)~(b). The figures demonstrate that the peak discharge conforms to a log - normal distribution with a mean of 6.19 and a standard deviation of 0.61. Subsequently, by taking into account the uncertainties in parameters such as λ_s , K_2 , K_3 ,n, s, a, and w with reference to existing literature**(Wu et al. 2024)**, the probability density distribution of the scour depth was fitted through Monte Carlo simulation. As shown in Fig.5(c), the results suggest that it is reasonable to represent the randomness of the scour depth using a log - normal distribution.

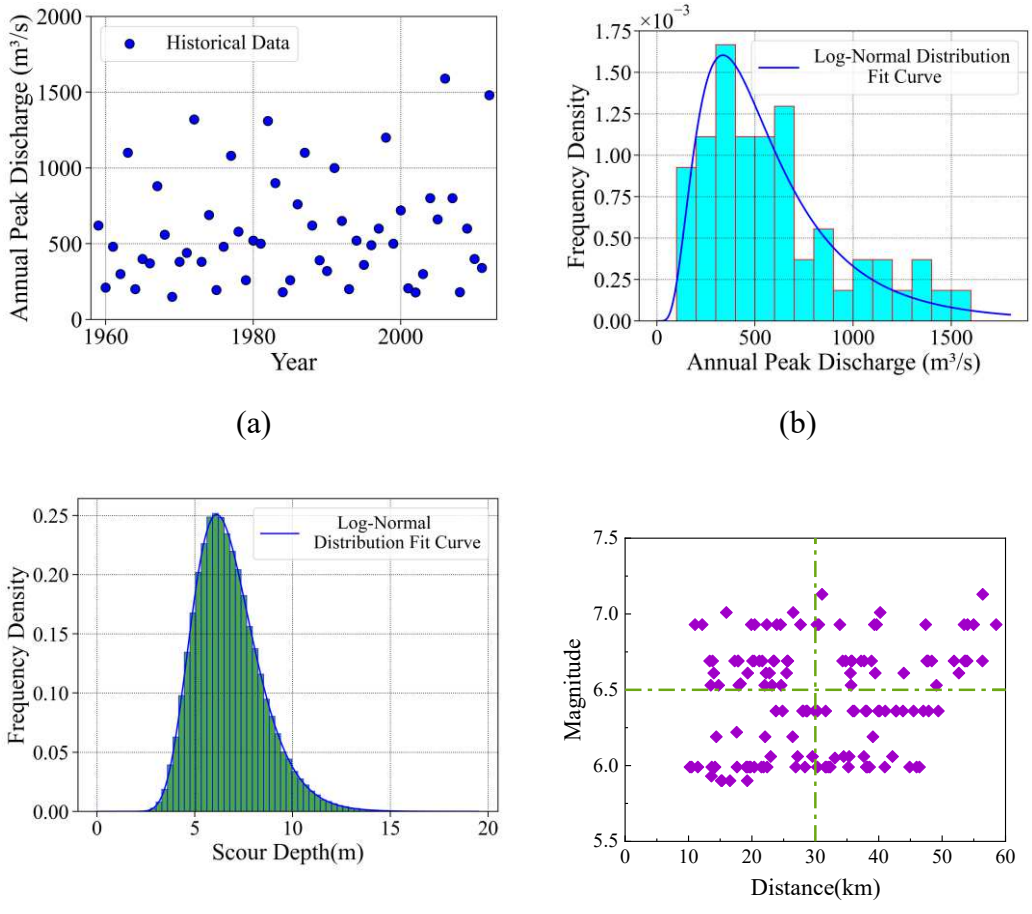


Fig.5 Uncertainty distribution of floods and ground motions considered in this study: (a) Historical flow records; (b) Historical flow; (c) Scour depth; (d) Magnitude and distance.

Furthermore, to obtain ground motion input data with a wide range of variation, this study selected 140 sets of far-field random ground motion data collected in previous research **(Yao 2023)** to simulate the randomness of input records. The corresponding distribution of magnitude and distance for theses ground motion are shown in **Fig.5(d)**. The ground motion input method in the OpenSees model was simultaneous bidirectional input in the longitudinal and transverse directions. Although previous research indicates that the Spectral Acceleration (SA) corresponding to the structure's fundamental period is more suitable as the Intensity Measure (IM) for the seismic fragility analysis of small and medium-span bridges**(Padgett et al. 2008; Aljawhari et al. 2021; Jamdar et al. 2024)**, the consideration of random flood-induced scour in the present study leads to variations in the fundamental period of the bridge model under different scour conditions. The modal analysis shows that the first natural period increases from 0.670 s to 0.917 s as scour depth increases from 0 m to 15 m. Therefore, this paper adopts Peak Ground Velocity (*PGV*) as the IM for the bridge seismic fragility analysis.

3.4 Output Parameters and Uncertainties

The selection of output parameters is another significant critical variable that need to be identified in machine learning analysis. In addition, their damage indices are used to measure the damage state of structures or components. These indices are related to the Engineering Demand Parameters (*EDPs*) in seismic fragility analysis. In bridge seismic fragility analysis, structural damage is typically classified into four levels: Slight Damage (*DS1*), Moderate Damage (*DS2*), Extensive Damage (*DS3*), and Complete Damage (*DS4*). Since piers, bearings, abutments, and scoured pile foundations are all vulnerable parts in the seismic design of bridges**(Wu et al. 2024; Wu et al. 2025)**, this study selects the curvature ductility ratio of pier and pile sections (μ_ϕ), the she μ_d is strain of pier bearings (γ), the displacement ductility ratio of abutment bearings (), and the displacements of the abutment in the active and passive directions ($\delta_{\text{Abut_}activ}$, $\delta_{\text{Abut_pass}}$) as the output parameters and *EDPs*. The corresponding damage indices are listed in Table 3. Meanwhile, with reference to existing research**(Li et al. 2024; Wu et al. 2025)**, the uncertainty in the seismic capacity of different components is considered, as shown in **Table 3.**

Table 3. Uncertainty and seismic capacity of different components at four damage states

Output	Component Name	EDP(Unit)	DS1		DS2		DS3		DS4	
			s_c	β_c	s_c	β_c	s_c	β_c	μ_d	β_c

Y1	Curvature ductility of pier top	$\mu_{\text{pier_T}}(/)$	1	0.127	1.35	0.247	6.48	0.321	11.16	0.383
Y2	Curvature ductility of pier bottom	$\mu_{\text{pier_B}}(/)$	1	0.127	1.32	0.247	5.86	0.321	11.13	0.383
Y3	Curvature ductility of foundation	$\mu_{\text{pile}}(/)$	1	0.127	1.27	0.247	4.62	0.321	10.27	0.383
Y4	Radial displacement ductility of pier bearing	$\mu_{pier_rad}(/)$	1	0.246	1.5	0.246	2	0.472	2.5	0.472
Y5	Tangential displacement ductility of pier bearing	$\mu_{pier_\tan}(/)$	1	0.246	1.5	0.246	2	0.472	2.5	0.472
Y6	Radial shear strain of abutment bearing	$\gamma_{abut_ran}(/)$	1	0.246	1.5	0.246	2	0.472	4	0.472
Y7	Tangential shear strain of abutment bearing	$\gamma_{abut_\tan}(/)$	1	0.246	1.5	0.246	2	0.472	4	0.472
Y8	Displacement of abutment in active direction	$\delta_{\text{abut_act}}(\text{mm})$	13	0.246	26	0.246	78	0.472	150	0.472
Y9	Displacement of abutment in passive direction	$\delta_{\text{abut_pas}}(\text{mm})$	5.5	0.246	11	0.246	35	0.472	100	0.472

4. Parameterized Multidimensional fragility Function of Bridges

4.1 PSDM and MPSDM

In seismic fragility analysis, the Probabilistic Seismic Demand Model (PSDM) is a crucial tool for assessing the relationship between structural response and seismic intensity. Traditional PSDM methods typically employ a log-linear regression model, which approximates the relationship between the seismic demand parameter (*EDP*) and the intensity measure (*IM*) through fitting, as expressed by the following approximate formula:

$$EDP = a(IM)^b \quad \text{or} \quad \ln EDP = \ln a + b \ln IM \tag{14}$$

where a and b are the regression coefficients. The parameter $\beta_{EDP|IM}$ is evaluated based on the statistical analysis of $\ln EDP$ and $\ln IM$:

$$\beta_{EDP|IM} = \sqrt{\frac{1}{N-2}\sum_{i=1}^{N}\left[\ln(EPD_i) - \ln(IM)\right]^2} \tag{15}$$

where, EDP_i is the demand from the ith ground motion input, and N is the number of dynamic time-history analyses. The aforementioned traditional PSDM has its limitations. This paper employs the Support Vector Regression (SVR) method to establish a multidimensional probabilistic seismic demand model (MPSDM). The input features for this model not only include the *IM* but also introduce other influencing factors, such as scour depth, incidence angle, and structural parameters. The SVR-based *EDP* predicted model *f(x)* can be calculated as:

$$f(x)=\sum_{i=1}^{N}\alpha_i K(x_i,x)+b \tag{16}$$

where *K(xi, x)* is the kernel function, *xi* denotes the input features, α_i and b are parameters of the support vector machine. Through nonlinear mapping, the SVR can effectively capture the complex nonlinear relationships among input features, thereby enhancing the model's prediction accuracy and adaptability. Compared to traditional regression-based PSDM, the SVR-based MPSDM can handle a greater number of input parameters and does not rely on linear assumptions. This enables the SVR method to better describe the structural response of bridges under the combined effects of multiple hazards and various uncertainty factors. By training with SVR, the complex relationships between each input feature and the seismic demand parameters can be obtained.

To ascertain the optimal dataset size for the development of the Support Vector Regression (SVR)-based multidimensional probabilistic seismic demand model (MPSDM), a convergence analysis was initially performed with four incrementally augmented sample sizes: *N*=560, 840, 1120, and 1400. **Fig. 6** illustrates the predictive performance of the SVR model for the nine engineering demand parameters (*EDPs*), evaluated using the coefficient of determination ($R^{2)}$ and the root mean square error (*RMSE)*. R^2 measures the proportion of variance in the sample data accounted for by the model, with values approaching unity indicating superior model fit. RMSE quantifies the average magnitude of deviation between predicted and observed values, where lower values correspond to reduced prediction errors.

$$R^2=1-\frac{\sum_{i=1}^{N}(y_i-\hat{y}_i)^2}{\sum_{i=1}^{N}(y_i-\bar{y}_i)^2} \tag{17}$$

$$RMSE=\sqrt{\frac{\sum_{i=1}^{N}(y_i-\hat{y}_i)^2}{N}} \tag{18}$$

where y_i represents the actual value of the sample, $\hat{y}_i$ represents the model's predicted value, $\bar{y}_i$ represents the sample mean, and n is the number of samples. Generally, a higher R^2 and a smaller *RMSE* indicate superior model prediction performance.

The overall prediction accuracy improves while the prediction error decreases when the sample size increases from 560 to 1400, indicating that the additional samples substantially enhance the learning capability of the SVR model in the high-dimensional parameter space. Similarly, **Soleimani (2022)** employed 960 simulation samples for fragility modeling involving 36 uncertain input parameters and demonstrated satisfactory prediction accuracy. Considering that the present study involves a larger uncertainty space with 39 random

input variables, including stochastic scour depth, curvature radius, and seismic incidence angle, a relatively larger data set is required to ensure sufficient coverage of the parameter domain and reliable nonlinear mapping between inputs and seismic responses. Therefore, a total of 1400 bridge-analysis samples were finally selected to establish the database of the proposed SVR-based MPSDM. Each sample consists of one set of input parameters and the corresponding *EDPs* obtained from nonlinear time-history analysis. The dataset was divided into two parts referring to a previous study**(Wang 2024)**: 90% of the samples were used for model training, while the remaining 10% were reserved as an independent test set. During model development, Bayesian optimization was performed on the training dataset, and 5-fold cross-validation was adopted as the internal validation procedure for hyper-parameter tuning and model selection.

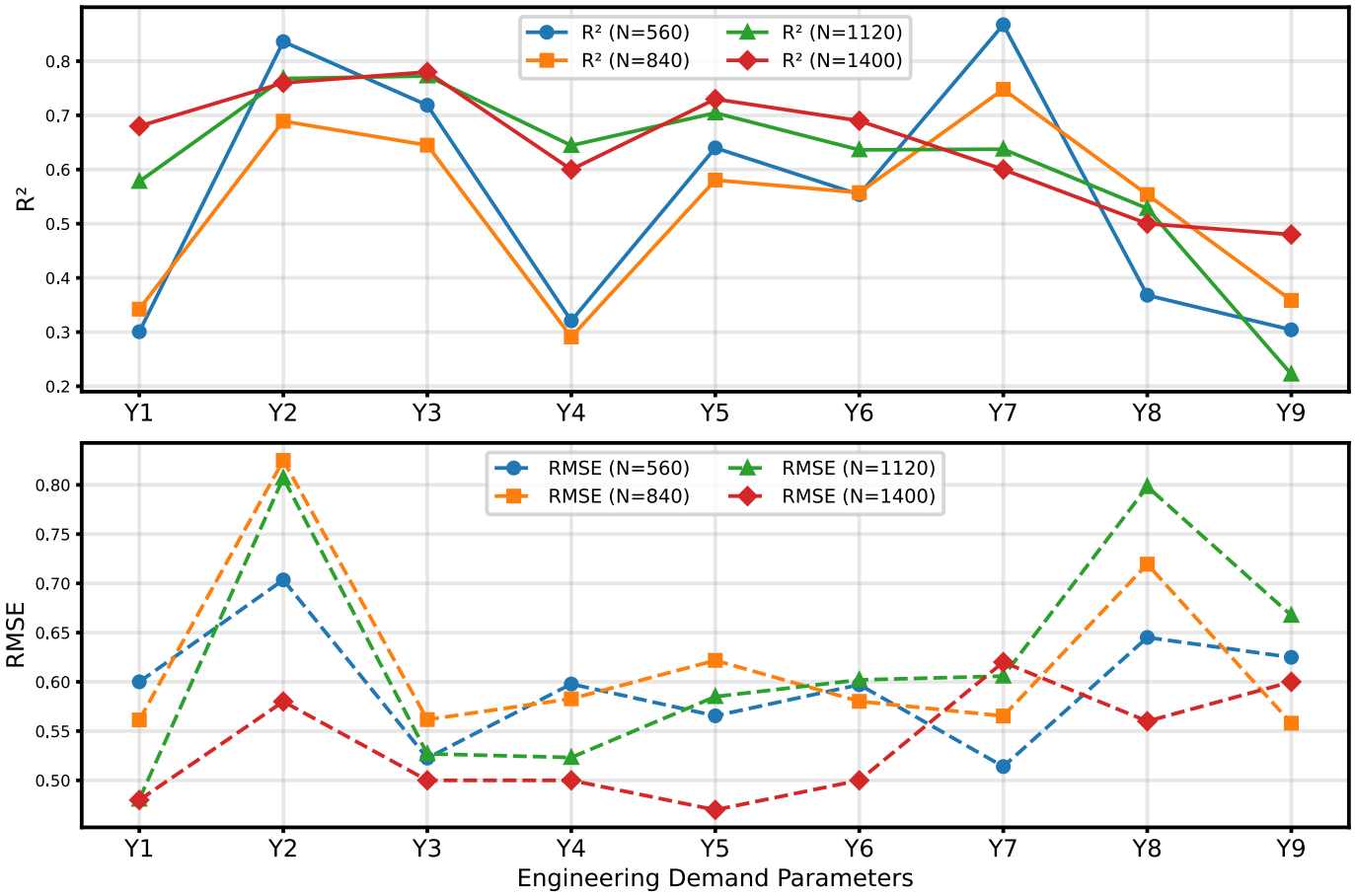


Fig.6 Convergence analysis of the SVR model under different training sample sizes.

4.2 Hyper-parameter Optimization of the SVR Algorithm

The establishment of an SVR model largely depends on its hyper-parameters, which determine the model's generalization and learning abilities. In this study, when constructing the SVR model, the Radial Basis Function (RBF) is employed as the kernel function to characterize the complex nonlinear relationship between the input variables and the Engineering Demand Parameters (*EDPs*). To enhance the generalization ability of the Support Vector Regression model, the Bayesian optimization method is used to automatically search for

the optimal penalty coefficient (C), kernel function parameter (γ), and epsilon-insensitive loss parameter (ε). The 5-fold cross-validation mean squared error (CV_MSE) is adopted as the objective function. The evaluation results from each iteration during the hyper-parameter search are recorded, and the convergence curve of the objective function is plotted, as shown in **Fig. 7**. Simultaneously, the optimal hyper-parameter combinations and corresponding model performance metrics for the nine *EDPs* listed in **Table 3** are extracted, as presented in **Table 4**. It can be observed from **Fig. 7** that as the number of function evaluations increases, the historical optimal objective value gradually decreases and stabilizes. This indicates that the Bayesian optimization method employed in this study can effectively search for a superior combination of SVR hyper-parameters.

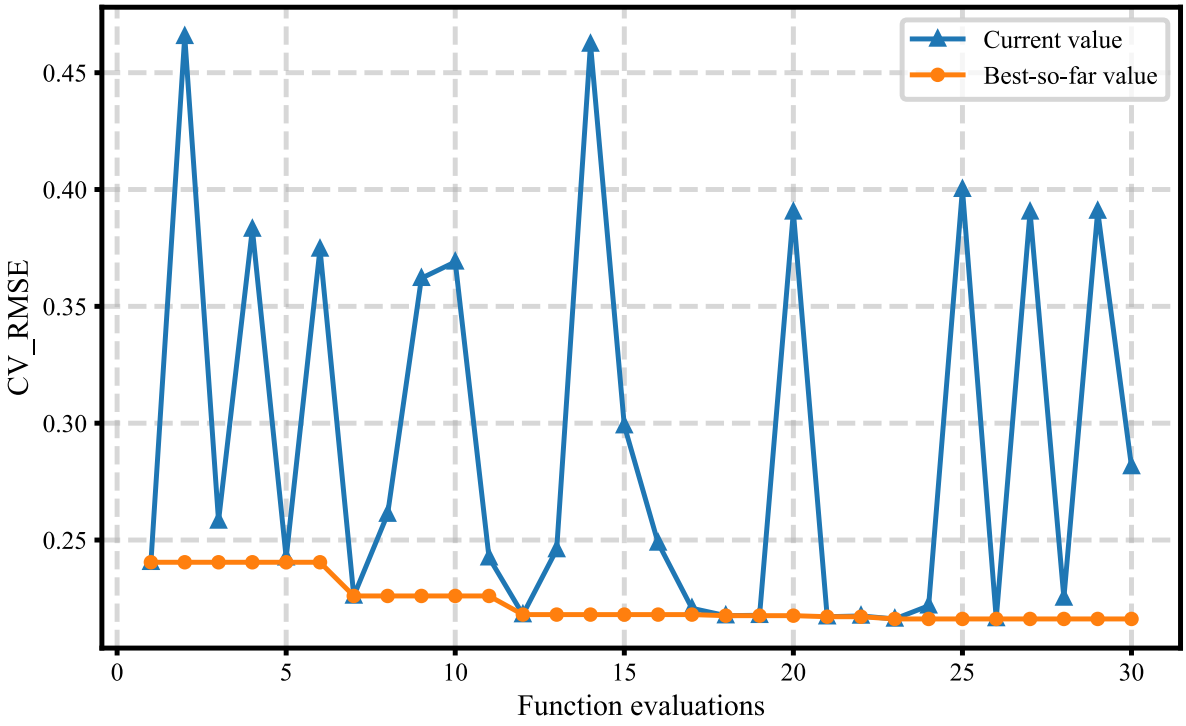


Fig.7 Hyper-parameter optimization process of SVR model

Table 4. Optimal Hyper-parameters of the developed SVR model

Output	C	ε	γ	CV_RMSE
Y1	40.46	0.0042	0.0025	0.24
Y2	21.66	0.0010	0.0017	0.21
Y3	1000.00	0.1189	0.0001	0.21
Y4	985.88	0.0744	0.0004	0.16
Y5	192.20	0.0024	0.0006	0.19
Y6	1000.00	0.0579	0.0001	0.16
Y7	1000.00	0.0037	0.0003	0.22

Y8	1000.00	0.0404	0.0001	0.17
Y9	475.38	0.0258	0.2525	0.18

4.3 Validation of the SVR-Based PSDM

To further validate the effectiveness of the established machine learning MPSDM, this study employs the coefficient of determination R^2 and the root mean square error RMSE as evaluation metrics. Generally, a higher R^2 and a smaller *RMSE* indicate superior model prediction performance. **Fig. 8** presents a comparison of and *RMSE* between the traditional linear PSDM and the SVR-based multidimensional PSDM for nine response indicators: curvature at pier top, curvature at pier bottom, curvature of pile foundation, radial displacement of pier bearing, tangential displacement of pier bearing, radial displacement of abutment bearing, tangential displacement of abutment bearing, active displacement of abutment, and passive displacement of abutment. The results indicate that the SVR model achieves higher R^2 and lower *RMSE* across all components compared to the traditional linear PSDM, demonstrating that SVR possesses better fitting capability and higher prediction accuracy. The improvement is most pronounced for components 8 and 9, indicating that for component responses with stronger nonlinear characteristics, the traditional linear PSDM struggles to accurately capture the variation pattern of their demands, whereas the SVR model can more effectively capture the complex mapping relationships under the coupling effects of multiple parameters. Therefore, the multidimensional PSDM constructed based on SVR is more suitable for the subsequent seismic fragility analysis in this study.

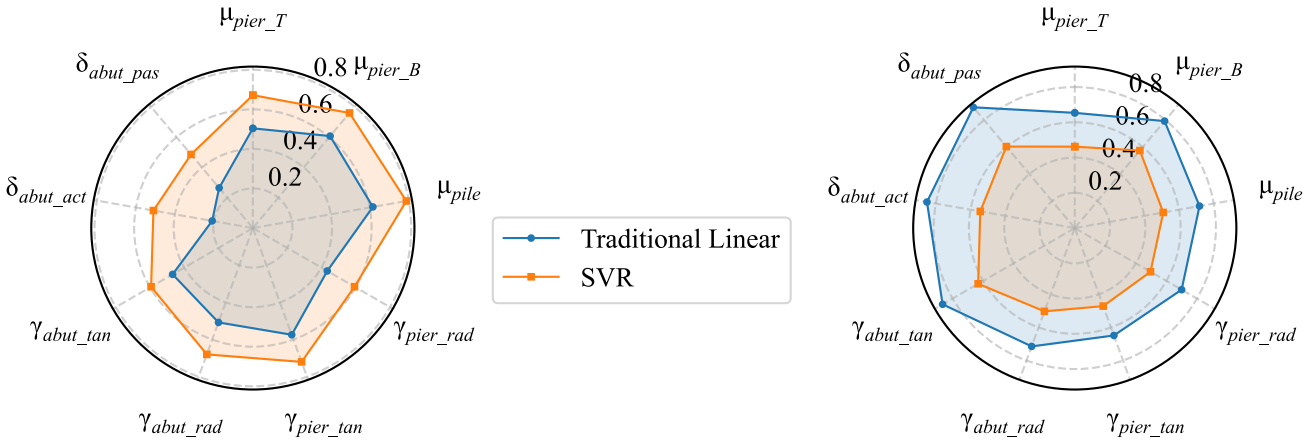


Fig.8 Comparison of the predictive performance of traditional PSDM and LM PSDM: (a) Coefficient of Determination (R^2); (b) Root Mean Square Error (RMSE).

In addition to the improved predictive accuracy indicated by higher R^2 and lower *RMSE*, the trained SVR-based MPSDM can serve as a surrogate demand model for rapid fragility evaluation under different parameter combinations. This avoids rerunning nonlinear time-history analyses for each individual scenario and is therefore particularly suitable for multi-parameter fragility surface construction. It should be noted that the purpose

of this comparison is not to establish the universal superiority of SVR over all nonlinear surrogate models, but to demonstrate that an SVR-based multidimensional PSDM provides an effective nonlinear alternative to the conventional linear PSDM for the present fragility problem.

4.4 SVR-Based Multi-parameter fragility Model

Based on the established SVR-based MPSDM, a multi-parameter parameterized seismic fragility model of RC curved bridges is further constructed. Different from the analytical methods in traditional fragility analysis, which are based on log-linear demand models and preset probability distributions, this study employs SVR to establish a nonlinear mapping relationship between the input parameters and the *EDPs*. Combined with Monte Carlo random sampling, the probability of the structure reaching or exceeding a given damage state under different parameter combinations is estimated, thereby constructing seismic fragility surfaces that consider the influence of factors such as scour depth, curvature radius, and seismic input angle. The input feature vector **X** is expressed as follows:

$$\mathbf{X} = [X_1, X_2, \ldots, X_{35}, H_s, R, \theta, IM] \quad (19)$$

where, H_S represents the scour depth, R represents the curvature radius, θ is the seismic input angle, IM is the ground motion intensity measure, and $[X_1, X_2, \ldots, X_{35}]$ are the bridge structural random parameters. Based on the trained SVR model, the seismic demand prediction function can be established as:

$$\ln(EDP) = f_{(SVR)}(\mathrm{X}) \quad (20)$$

When the predicted demand, *EDP*, exceeds the capacity threshold corresponding to a specific damage state C_{ds_k}, the structure reaches or exceeds the *k*th damage state:

$$EDP \geq C_{ds_k} \quad (21)$$

Under a given combination of control parameters, the Monte Carlo method is employed to sample the remaining random variables. The samples are then input into the SVR model to obtain the corresponding demand values, subsequently enabling the statistical calculation of the failure probability:

$$P(DS \geq DS_k \mid Z) = \frac{1}{N}\sum_{j=1}^{N} I\left[EDP^{(j)} \geq C_{ds_k}\right] \quad (22)$$

where, Z denotes different parameter combinations, N is the number of sampling iterations, and $I[\cdot]$ is the indicator function, which takes the value 1 if the condition inside the brackets holds true, and 0 otherwise. By repeating the aforementioned process within the parameter space, the exceedance probabilities for each damage state under different parameter combinations can be obtained, enabling the further construction of multi-parameter seismic fragility surfaces. **Fig. 9** displays the developed fragility surfaces for the abutment bearings

in the tangential direction under varying scour depths (H_s), seismic input angles (θ), and curvature radius (R). Compared to traditional one-dimensional fragility curves, this method can more intuitively reveal the coupling effects of parameters such as scour depth, curvature radius, and seismic input angle on the damage probability of bridges.

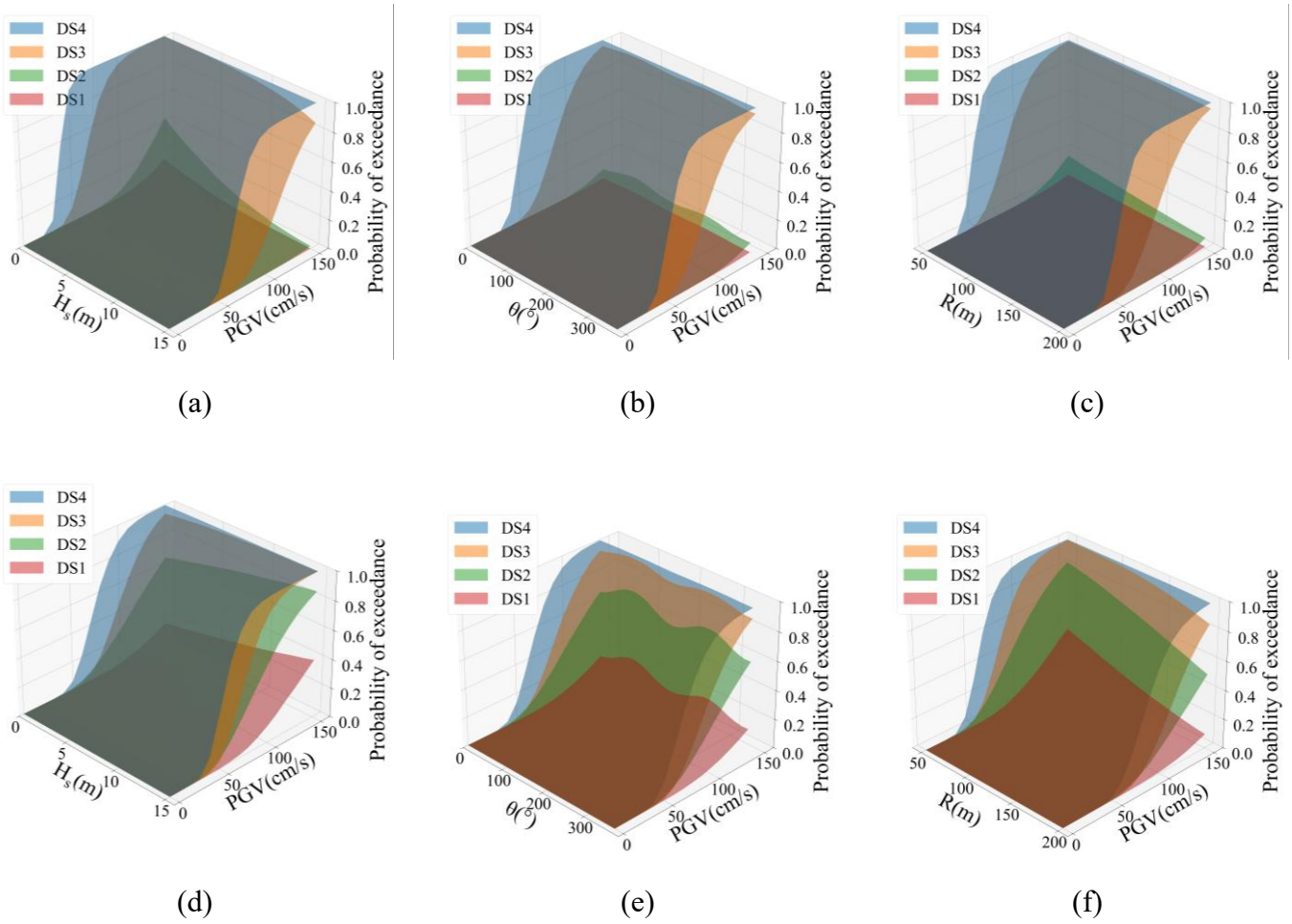


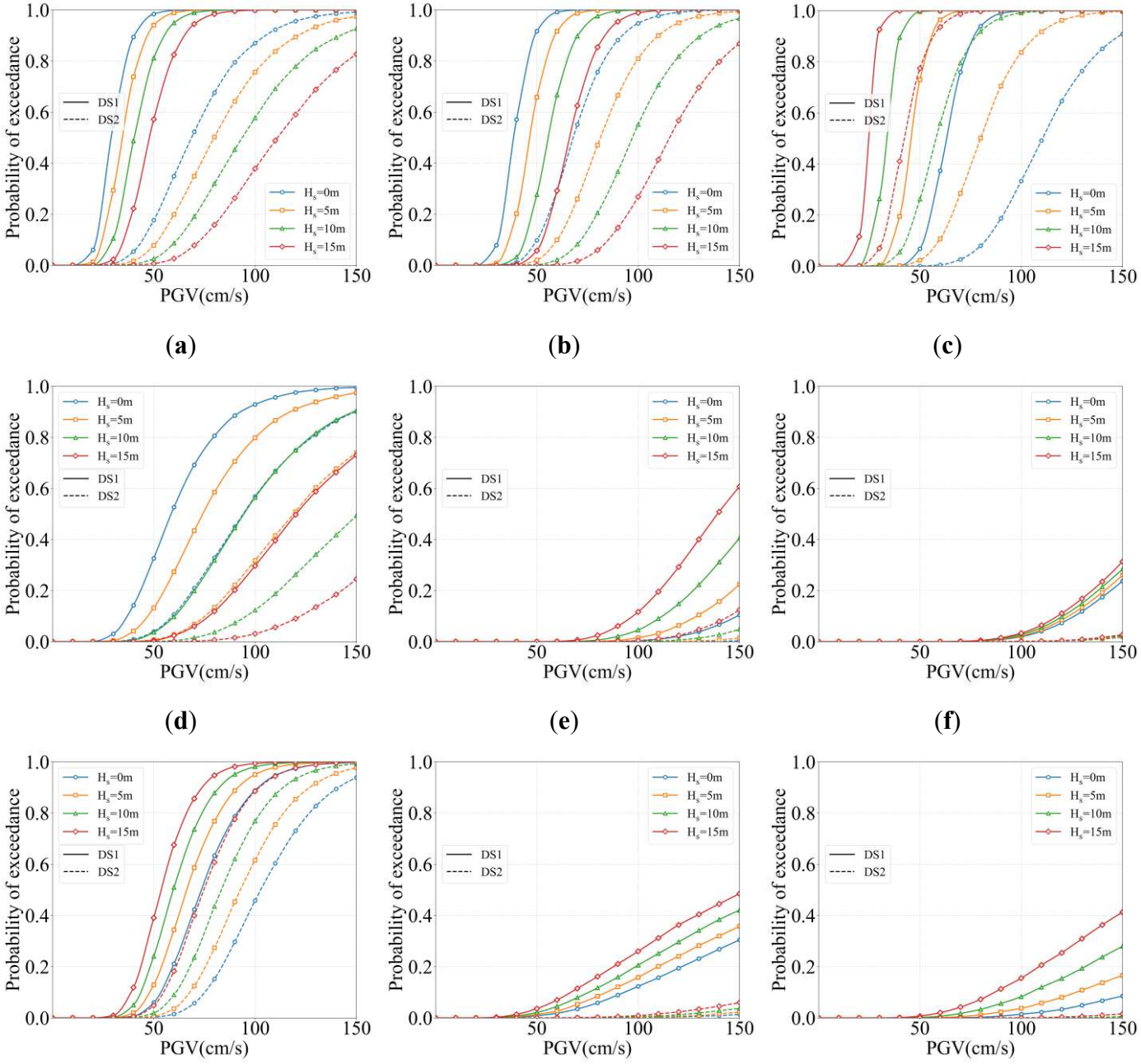
Fig.9 Seismic fragility surfaces of pier and abutment bearing under different conditions: (a) Pier-Hs; (b) Pier-θ; (c) Pier-R; (d) Abutment Bearing-Hs; (e) Abutment Bearing-θ; (f) Abutment Bearing-R.

In summary, the developed SVR-based multi-parameter fragility model in this study integrates the efficient nonlinear fitting capability of machine learning with the probabilistic estimation power of Monte Carlo simulation. It enables the estimation of the probability of a bridge reaching or exceeding a given damage state under different parameter combinations. Based on this model, subsequent chapters will present the bridge seismic fragility curves under varying conditions of scour depth, curvature radius, and seismic input angle, and analyze the influence patterns of each parameter on the structural damage probability.

5. Impact of Different Parameters on the Seismic fragility

5.1 Impact Analysis of Scour Depth

To examine the influence of scour depth on the seismic fragility of parameterized RC curved bridges, four representative scour conditions with *Hs* values of 0, 5, 10, and 15 m were selected. While keeping all other parameters constant, fragility curves were developed for nine response indicators under both slight damage (*DS1*) and moderate damage (*DS2*), as depicted in **Fig.10**. The selected indicators encompass the curvature at the pier top and pier bottom, the curvature of the pile foundation, the tangential and radial displacement ductility ratios of the pier bearings, the tangential and radial displacement ductility ratios of the abutment bearings, and the maximum abutment displacements in the active and passive directions. These indicators were chosen to characterize the seismic fragility of the key components of the curved bridge.



(**g**) (**h**) (**i**)

Fig.10 Seismic ragility curves of pier column and abutment bearing under different conditions:(a) Pier_top; (b) Pier_bottom; (c) Pile; (d) Pier_bearing_rad; (e) Pier_bearing_tan; (f) Abutment_bearing_rad; (g) Abutment_bearing_tan; (h) Abutment_active; (i) Abutment_passive.

As depicted in **Fig. 10**, the responses of different components to variations in scour depth display substantial disparities. As the scour depth *Hs* increases, the fragility curves corresponding to the pier top, pier bottom, and the radial pier bearing undergo an overall right - ward shift. This implies that their failure probabilities under the same seismic intensity gradually decline. For instance, at a peak ground velocity (*PGV*) of 70 cm/s, the failure probability of the pier bottom under damage state 2 (*DS2*) decreases from 54.9% to 1.5% as the scour depth increases from 0 m to 15 m. Meanwhile, the failure probability of the radial pier bearing under damage state 1 (*DS1*) decreases from 69.3% to 6.4%, with reduction rates of 97.3% and 90.8% respectively. Conversely, the fragility curves corresponding to the pile foundation, tangential pier bearing, tangential abutment bearing, and the abutment displacement in the active and passive directions generally shift to the left. This indicates that the failure probabilities of these components increase notably with the deepening of scour. For example, at *PGV* = 70 cm/s, the failure probability of the pile foundation under *DS2* rises from 2.7% to 98.8%, and that of the tangential abutment bearing increases from 6.0% to 39.8% as the scour depth increases from 0 m to 15 m, representing increases of 96.1 and 33.8 percentage points respectively. In contrast, the radial displacement ductility ratio of the abutment bearing is less influenced by scour.

These findings suggest that as scour weakens the soil restraint around the foundation and enhances the overall structural flexibility, the damage demand is redistributed from some pier sections to displacement - controlled components, especially pile foundations, tangential bearings, and abutments. Specifically, the pier bearings demonstrate a differential characteristic of "decrease in the radial direction and increase in the tangential direction." The abutment bearings, on the other hand, exhibit a response pattern of "minor change in the radial direction and significant change in the tangential direction." This demonstrates that scour has inconsistent impacts on the responses of different bearings and directions in curved bridges. Overall, flood - induced scour causes a shift in the potential weak locations of parameterized reinforced concrete (RC) curved bridges, which is consistent with the findings reported by **Ganesh Prasad and Banerjee (2013), Wu et al. (2024)**, and **Hung and Yau (2017)**, who also demonstrated that scour-induced loss of foundation restraint may significantly alter structural demand distribution and amplify seismic fragility . Therefore, fragility analyses under the combined effects of scour and earthquake should give particular consideration to the damage risks of foundation and boundary components.

5.2 Impact Analysis of Seismic Input Angle

To examine the influence of the seismic input angle θ on the seismic fragility of parameterized reinforced concrete (RC) curved bridges, six representative response indicators were selected: the curvature at the pier bottom, the radial displacement ductility ratio of the pier bearing, the tangential displacement ductility ratio of the pier bearing, the radial displacement ductility ratio of the abutment bearing, the tangential displacement ductility ratio of the abutment bearing, and the maximum displacement of the abutment in the active direction. fragility surfaces for different damage states under the combined action of peak ground velocity (PGV) and the input angle were established for these indicators, as shown in **Fig. 11**. Furthermore, to further clarify the angular dependence of representative components, the failure probabilities at PGV = 70 cm/s were presented in polar form in **Fig. 12**. The selected components represent the main response of the pier, the connection response of the bearings, and the boundary response of the abutment, which can comprehensively reflect the impact of the seismic input direction on the damage probability of key parts of the curved bridge.

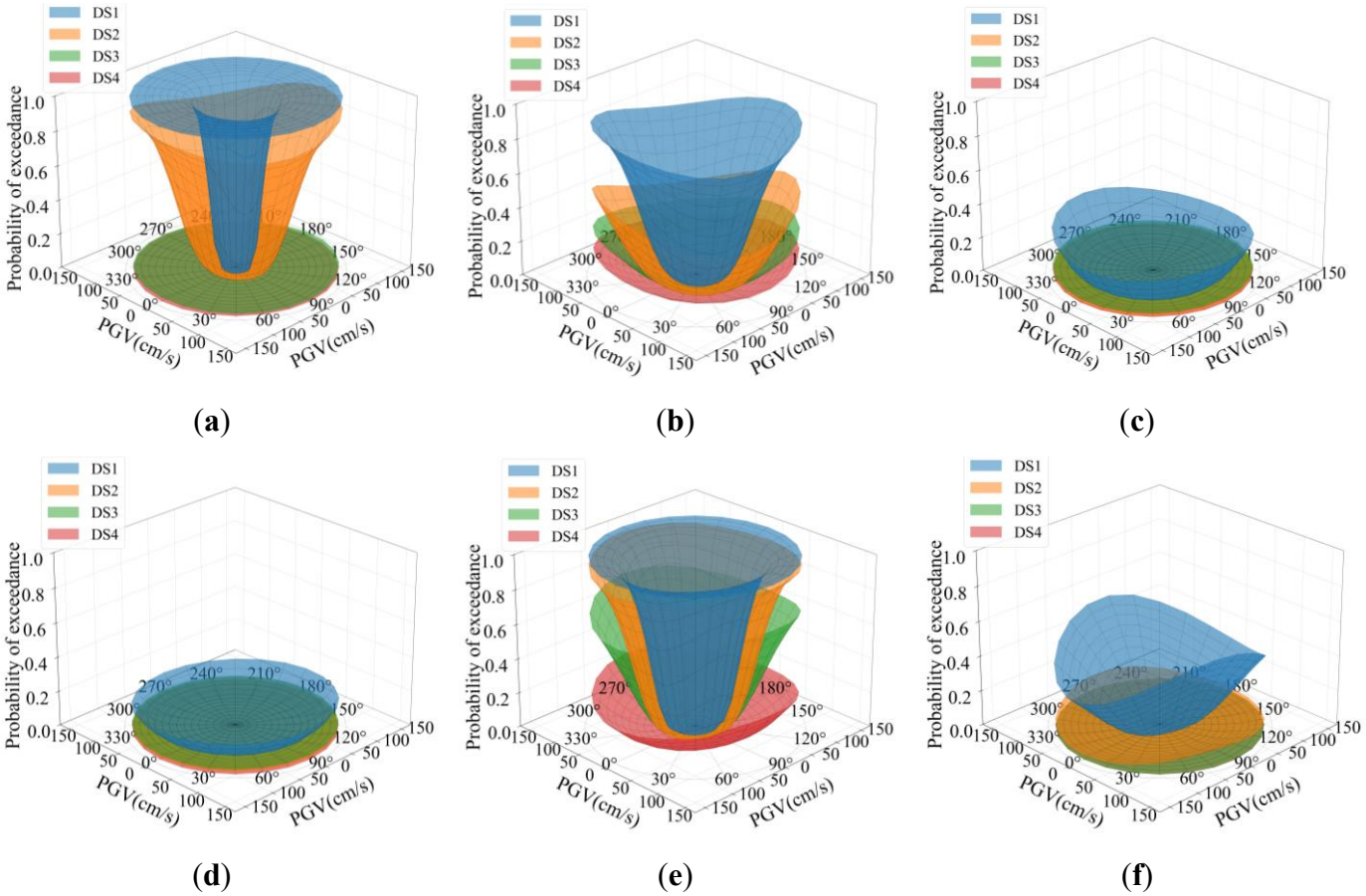


Fig.11 The impact of varying earthquake input angles on the seismic fragility of bridge components: (a) Pier_top; (b) Pier_bearing_rad; (c) Pier_bearing_tan; (d) Abutment_bearing_rad; (e) Abutment_bearing_tan; (f) Abutment_active.

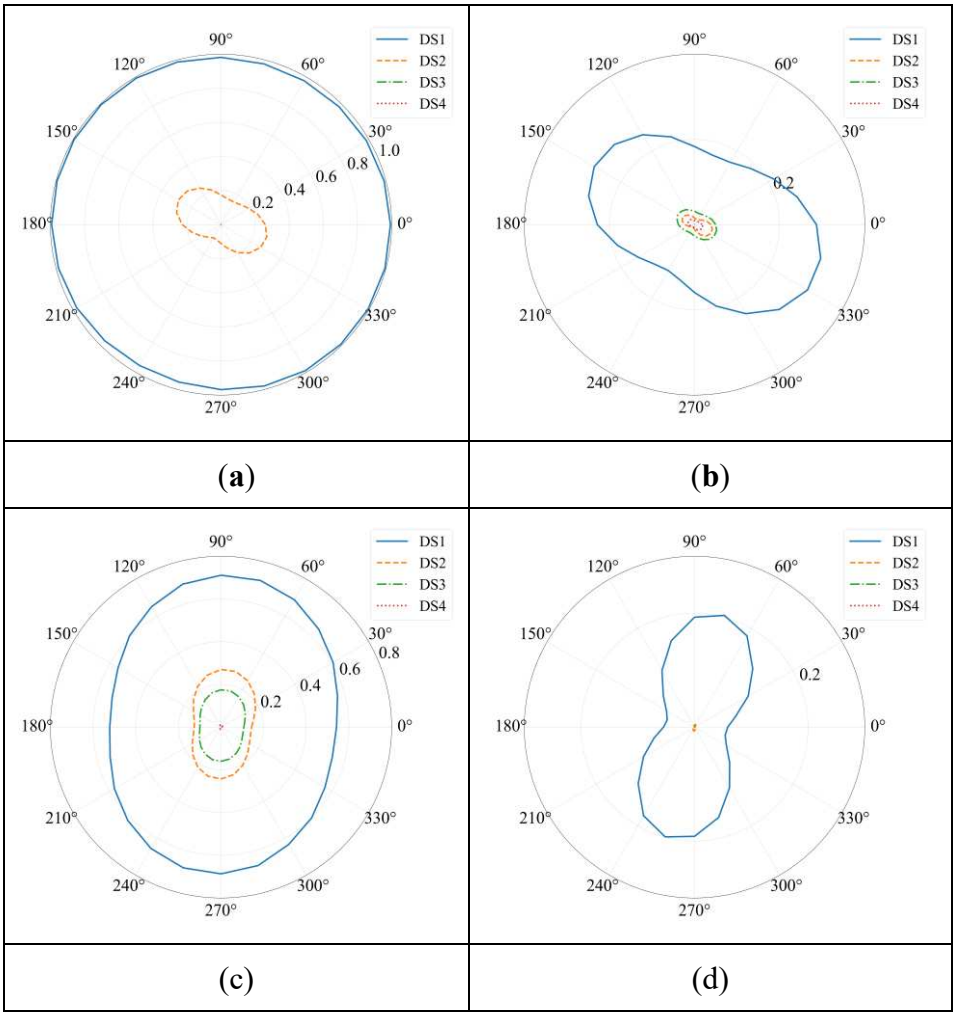


Fig.12 Failure probability versus seismic incidence angle for representative components at PGV=70cm/s: (a) Pier Top; (b) Pier Bearing; (c) Abutment Bearing; (d) Abutment Active.

As depicted in **Fig. 11**, the sensitivity of different components to the seismic input angle θ varies significantly. The failure probability of the pier exhibits minimal variation with the input angle. Although its sensitivity to the excitation orientation increases as the limit state rises, the overall influence of the input direction on the pier response remains limited. In contrast, the bearings and abutments are more sensitive to the input angle and display a distinct most unfavorable incidence direction. Among them, the radial pier bearing varies considerably with θ across different damage states, with the most unfavorable input angles mainly around 150° and 330°. The failure probability corresponding to the tangential pier bearing is relatively small and is less affected by the input angle. The abutment bearings show different patterns. The tangential abutment bearing corresponds to a higher failure probability and is more sensitive to the input angle, with the most unfavorable angles concentrated mainly around 90° and 270°. The displacement of the abutment is also notably affected by the input angle, and its most adverse direction is also approximately 90° and 270°.Thesensitivity of bearings and abutments to seismic incidence angle agrees with previous studies **(Feng et al. 2018; Rashid and Nishio**

2025; Tehrani and Heydarpour 2025), which also identified the earthquake input direction as an important factor governing the seismic response of curved bridges.

The aforementioned findings suggest that the seismic input angle exerts a substantial influence on the damage risk of boundary components, including bearings and abutments, by modifying the in - plane response characteristics of the curved bridge. In contrast, its impact on the pier response is relatively restricted. Consequently, in the seismic fragility analysis of curved bridges, the effect of the input angle should be fully taken into account, with special attention being paid to controlling the damage of bearings and abutments under the most adverse input directions.

5.3 Impact Analysis of the Curvature Radius

To analyze the influence of the bridge curvature radius R on the seismic fragility of parameterized reinforced - concrete (RC) curved bridges, four representative cases with R = 50, 100, 150, and 200 m were taken into consideration. While keeping all other parameters constant, the fragility curves for the nine key components under different curvature radii were separately plotted, as depicted in **Fig. 13**. **Fig. 13** shows that as the curvature radius R increases, the fragility curves of all components generally shift rightward. This implies that a larger curvature radius can decrease the failure probability of parameterized RC curved bridges under seismic action, though the sensitivity of different components varies. The influence of curvature radius observed in this study is also consistent with earlier investigations by previous studies **(Tondini and Stojadinovic 2012; Jeon et al. 2016; Jiao et al. 2018)**, which reported that smaller curvature radii generally lead to stronger irregular response and higher seismic demand. The curvature at the pier top, curvature at the pier bottom, and curvature of the pile foundation are relatively less affected by changes in the curvature radius, with the damage probabilities under different radii being quite comparable. In contrast, the responses associated with bearings and abutments are more significantly influenced by variations in the curvature radius. For the pier bearings, the damage probability corresponding to the radial displacement is greater than that of the tangential displacement, and the radial response is more sensitive to changes in the curvature radius. For the abutment bearings, the failure probability in the tangential direction is generally higher than that in the radial direction, and both are significantly affected by variations in the curvature radius. In particular, under strong ground motions, the radial damage of the abutment bearings is more sensitive to the curvature radius. For instance, at a peak ground velocity (PGV) of 150 cm/s, as the curvature radius increases from 50 m to 200 m, the failure probability of the radial abutment bearing decreases significantly from 48.0% to 3.7%, corresponding to a relative reduction

of approximately 92.3%. Regarding abutment displacement, the damage probability corresponding to the active direction is generally greater than that in the passive direction. Overall, the results suggest that an increase in the curvature radius can, to a certain extent, alleviate the spatial response effects induced by the plan irregularity of curved bridges. This influence is mainly manifested in the boundary and connection components, such as bearings and abutments.

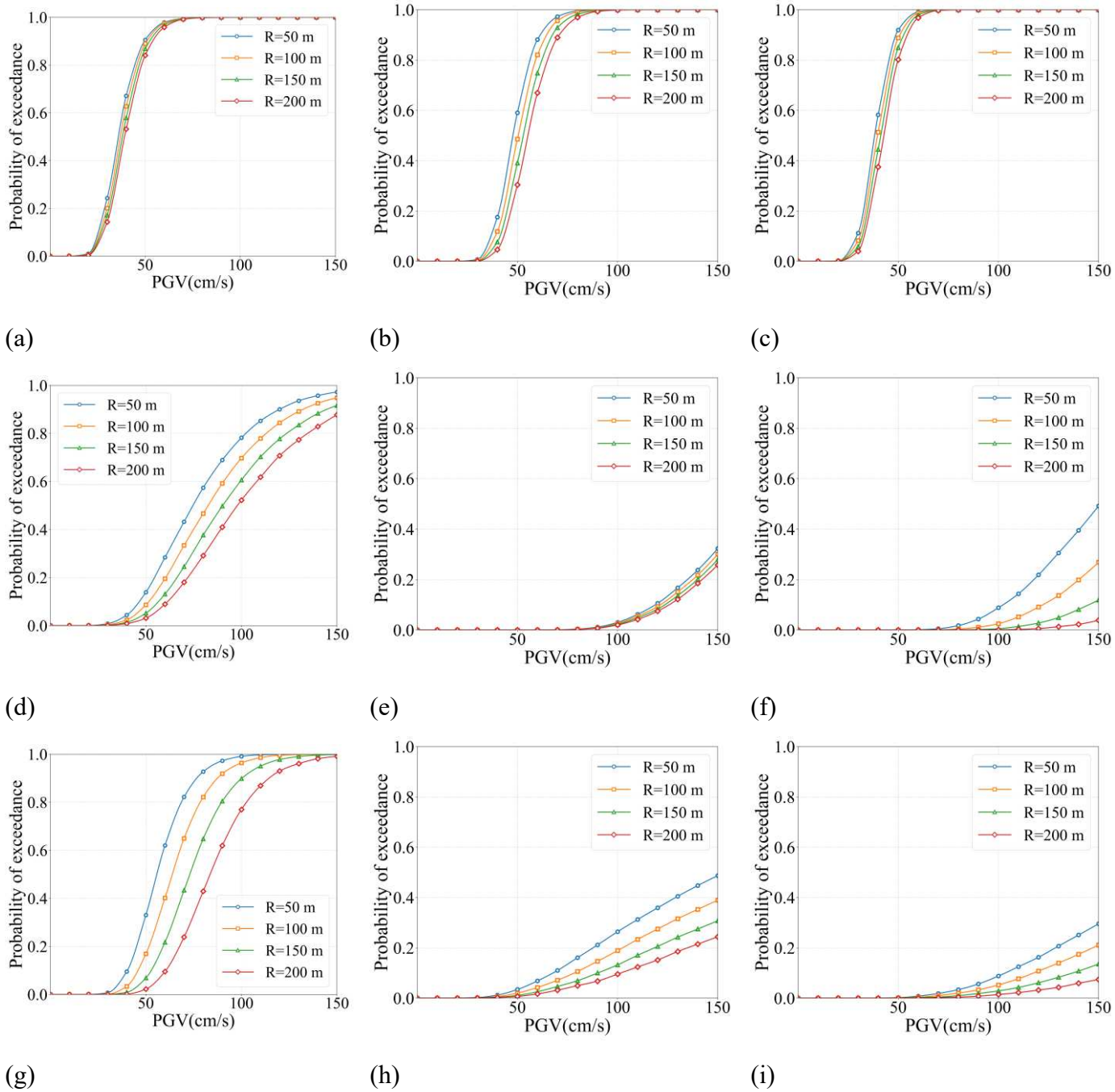


Fig.13 The impact of varying curvature radii on the seismic fragility of bridge components: (a) Pier_top; (b) Pier_bottom; (c) Pile; (d) Pier_bearing_rad; (e) Pier_bearing_tan; (f) Abutment_bearing_rad; (g) Abutment_bearing_tan; (h) Abutment_active; (i) Abutment_passive.

5.4 Coupled Effects of Different Parameters

To further clarify the seismic fragility evolution of parameterized curved reinforced concrete (RC) girder bridges under multi - parameter interactions, the tangential displacement ductility ratio of the abutment bearing is selected as a representative index owing to its high sensitivity to parameter variations. At a peak ground velocity (*PGV*) of 80 cm/s, the joint effects of the curvature radius R and seismic input angle θ, the curvature radius R and scour depth H_s, and the seismic input angle θ and scour depth H_s are respectively discussed. **Fig. 14 - Fig.16** display the fragility comparisons for slight and moderate damage states.

The results reveal that, under fixed *PGV* and H_s conditions, the failure probability generally decreases as the curvature radius increases. Meanwhile, it shows significant fluctuations with the seismic input angle, reaching relatively high levels near 90° and 270°. This indicates a distinct coupling effect between the curvature radius and the seismic input angle. The curvature radius mainly affects the overall level of damage probability, and the input angle primarily determines its fluctuation pattern and the most unfavorable direction. Under different scour depth conditions, the failure probability decreases as the curvature radius increases. For the same curvature radius, it increases with the increase of the scour depth. This implies that a significant coupling effect also exists between the curvature radius and the scour depth. The combination of a small curvature radius and a large scour depth is more likely to form a high - risk scenario. Under different scour depth conditions, the failure probability shows significant fluctuations with the seismic input angle. For the same input angle, it generally increases with the increase of the scour depth. This suggests that the seismic input angle mainly controls the fluctuation characteristics of the damage probability along the angular direction, while the scour depth mainly raises its overall probability level.

In conclusion, the seismic fragility of parameterized RC curved bridges exhibits distinct multi - parameter coupling characteristics. The curvature radius, seismic input angle, and scour depth jointly govern the bridge damage risk and the distribution of unfavorable conditions. Bridge components under the combined scenario of a small curvature radius, a relatively large scour depth, and an unfavorable input direction are more prone to entering high - damage states. This combination should be a key focus in seismic design and risk assessment.

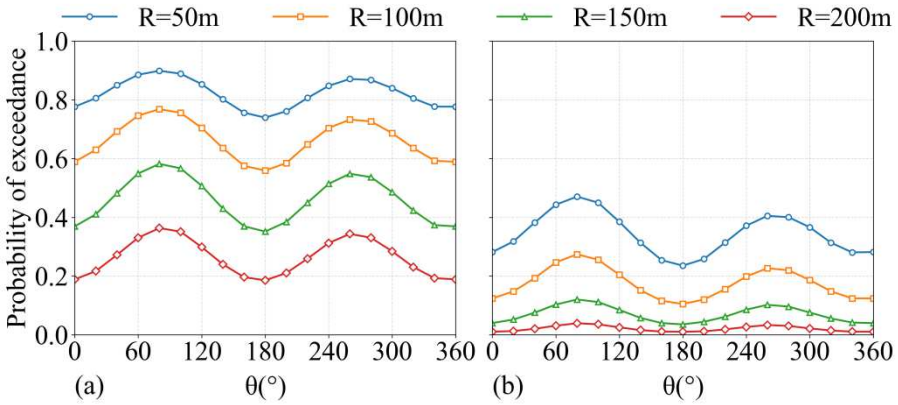


Fig.14 Comparison of the tangential damage probability of bridge abutment bearings with different curvature radii under various incidence angles: (a) DS1; (b) DS2.

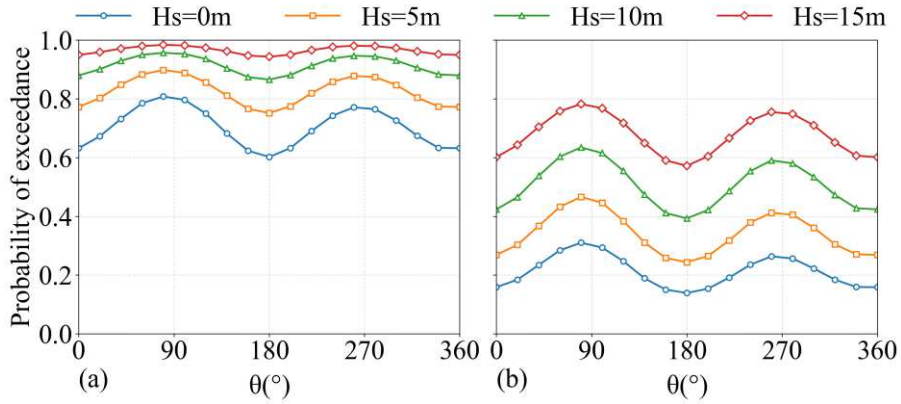


Fig.15 Comparison of damage probabilities of tangential displacement at abutment bearings under different incidence angles for different curvature radii: (a) DS1; (b) DS2.

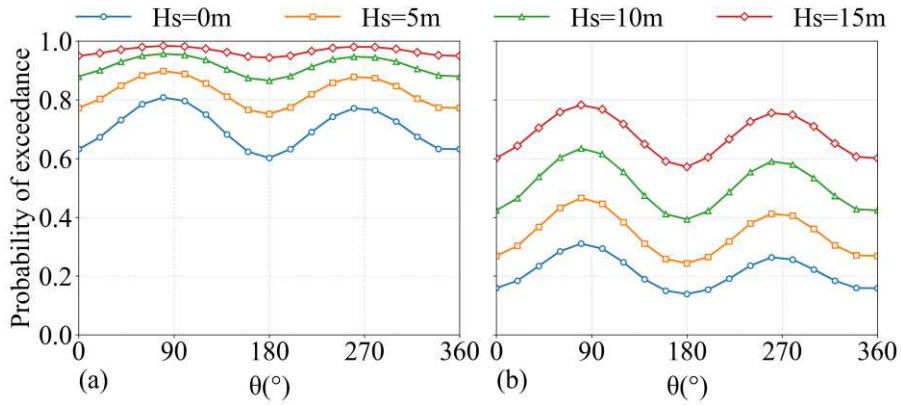


Fig.16 Comparison of damage probability of abutment bearings with different scouring depths under different incident angles: (a) DS1; (b) DS2.

6. Discussion

This research presents a seismic fragility analysis framework for curved bridges based on machine learning, taking into account the impacts of stochastic flood scour under the multi - hazard coupling of flooding and earthquakes. In contrast to traditional methods that characterize scour depth with a single extreme value,

the proposed framework explicitly incorporates the randomness of scour depth and its coupled effects with ground - motion intensity, seismic input angle, and bridge geometric parameters. This allows for a more precise evaluation of the damage risk of irregular curved bridges under complex environmental loading conditions.

With reinforced concrete (RC) curved bridges as the research subject, a parameterized finite - element model is established on the OpenSees platform. In this model, uncertainties in structural design, flood scour effects, and uncertainties in seismic input are comprehensively considered. Within this framework, the support vector regression (SVR) method is employed to construct a multidimensional probabilistic seismic demand model (PSDM) to capture the coupled nonlinear relationships between multiple input variables and bridge responses. Comparative analysis reveals that, for all key components, the SVR model attains higher R^2 values and lower root - mean - square error (RMSE) values compared to the traditional linear PSDM, indicating that it offers a more effective nonlinear surrogate for the current fragility problem. Moreover, based on the developed multidimensional PSDM, parametric fragility models are formulated under different random scour depths, ground - motion intensities, seismic input angles, and curvature radii. Although the present study focuses on the SVR model due to its strong generalization capability for medium-sized datasets and high-dimensional nonlinear problems, other nonlinear machine-learning models such as artificial neural networks, random forests, and gradient boosting methods may also provide competitive predictive performance. A comprehensive benchmark comparison among different surrogate models is an important topic for future research and could further optimize model selection for bridge fragility assessment problems.

Finally, by integrating the ML model with the LHS - based Monte Carlo simulation, the proposed framework enables the efficient estimation of bridge damage probabilities under various combinations of influencing parameters, eliminating the necessity of conducting repeated nonlinear time - history analyses for each scenario. The results demonstrate the applicability of the proposed framework in the performance assessment and risk - informed seismic evaluation of curved bridges in complex multi - hazard environments.

From an engineering perspective, the results suggest that the post - flood seismic assessment of curved bridges should consider not only piers but also pile foundations, tangential bearings, and abutment displacement. Where possible, bridges with small curvature radii should be avoided as they are more vulnerable to damage. In flood - prone regions, scour protection, foundation reinforcement, and post - flood inspection are particularly crucial when deep scour may coincide with unfavorable seismic input directions.

7. Conclusions

A multi - dimensional probabilistic seismic demand model for parameterized reinforced concrete (RC) curved bridges, which takes into account the effects of stochastic flood - induced scouring, was developed. The findings suggest that, in comparison with the traditional linear probabilistic seismic demand model (PSDM), the support vector regression (SVR) model demonstrates a higher coefficient of determination (R^2) and a lower root - mean - square error *(RMSE*). This enables a more precise depiction of the nonlinear variation in bridge seismic demands under multi - parameter conditions.

An increase in scour depth does not uniformly enhance the fragility of all structural components. Instead, it modifies the distribution of seismic demands among different parts of the structure. The damage probabilities associated with pier curvature and the radial displacement ductility ratio of pier bearings generally decline, while those for pile foundation curvature, the tangential displacement ductility ratios of bearings, and abutment displacements increase substantially. This implies that scouring causes a shift in the potential critical weak locations from certain pier sections to the foundations, the tangential direction of bearings, and the displacement - controlled zones at the abutments.

Both the seismic input angle and the curvature radius have a significant influence on the seismic fragility of parameterized RC curved bridges, yet the sensitivity varies among components. The pier response is less sensitive to changes in the input angle, whereas bearings and abutments are highly sensitive and display distinct most unfavorable incidence directions. As the curvature radius increases, the fragility of all key components decreases overall, with bearings and abutment - related responses being more sensitive to this change. This indicates that the curvature radius plays a crucial role in regulating the spatial response effects resulting from the plan irregularity of curved bridges.

Evident coupling effects exist among different parameters. When the curvature radius and seismic input angle act in combination, bridges with smaller curvature radii not only have higher overall damage probabilities but also exhibit greater fluctuation amplitudes with changing input angles. Under the combined effect of the curvature radius and scour depth, the amplifying effect of scouring on the damage probability of boundary components is more pronounced for bridges with smaller curvature radii. When the seismic input angle and scour depth act jointly, the impact of scouring on component damage probability varies significantly across different input directions and is more prominent near unfavorable incidence angles. This demonstrates that the seismic fragility of parameterized RC curved bridges exhibits distinct multi - parameter coupling characteristics. In engineering practice, high - risk scenarios involving a combination of a small curvature radius, a

relatively large scour depth, and an unfavorable input direction should be a key focus in seismic design and risk assessment.

Author contributions: Wenpeng Wu contributed to the study conception and design, and provided funding and supervision; Jiacheng Li and Jiqiu Zhou performed data collection and wrote the original draft; Xin Ye contributed to the study conception and analysis; Jiaqin Hou provided critical data and wrote comments; All authors reviewed and approved the final manuscript.

Funding: This study was financially supported by by the Hunan Provincial Natural Science Foundation of China through Grant No.2024JJ5380.

Declaration: The authors declare that they have no known competing financial interests or personal relationships that could have appeared to influence the work reported in this paper.

References

Abbasi M, Abedini MJ, Zakeri B, Ghodrati Amiri G (2016) Seismic vulnerability assessment of a Californian multi-frame curved concrete box girder viaduct using fragility curves. Structure and Infrastructure Engineering 12(12):1585-1601

Aljawhari K, Gentile R, Freddi F, Galasso C (2021) Effects of ground-motion sequences on fragility and vulnerability of case-study reinforced concrete frames. Bull. Earthquake Eng. 19(15):6329-6359

Annad M, Zourgui NH, Lefkir A, Kibboua A, Annad O (2023) Scour-dependent seismic fragility curves considering soil-structure interaction and fuzzy damage clustering: A case study of an Algerian RC Bridge with shallow foundations. Ocean Eng. 275:114157

Ansari A, El-Hussain I, Al Shijbi Y, Mandhaniya P, Alluqmani AE, Al-Jabri K (2024) Robustness assessment of Muscat coastal highway network (CHN) under multi-hazard scenarios focusing on traffic stability and adaptation measures. Scientific Reports 14(1):30632

Arneson LA, Zevenbergen LW, Lagasse PF, Clopper PE (2012) Evaluating Scour at Bridges. In: Federal Highway Administration, U.S. Department of Transportation, Washington, DC, USA

Ateş S, Avşar Ö (2023) The impact of ground motion incidence angle for skewed highway bridges under multi-hazard effects of scour and earthquake. In: 3rd International Civil Engineering have Architecture Congress. Trabzon, Türkiye

Ateş S, Avşar Ö (2024) Seismic performance of skewed bridges with uniform and non-uniform scour. Soil Dynamics and Earthquake Engineering 187:108976

Biazar S, Kameshwar S, Balomenos GP (2024) Multi-hazard fragility modeling framework for bridges with shallow foundations subjected to earthquake, scour, and vehicular loading. Soil Dyn. Earthquake Eng. 178:108482

Ding J-Y, Feng D-C, Brunesi E, Parisi F, Wu G (2023) Efficient seismic fragility analysis method utilizing ground motion clustering and probabilistic machine learning. Engineering Structures 294:116739

Feng R, Wang X, Yuan W, Yu J (2018) Impact of seismic excitation direction on the fragility analysis of horizontally curved concrete bridges. Bull. Earthquake Eng. 16(10):4705-4733

Ganesh Prasad G, Banerjee S (2013) The impact of flood-induced scour on seismic fragility characteristics of bridges. Journal of Earthquake Engineering 17(6):803-828

Ge B, Yang Y, Kim S (2023) Time-dependent multi-hazard seismic vulnerability and risk assessment of deteriorating reinforced concrete bridges considering climate change. Structures 55:995-1010

Guo X, Wu Y, Guo Y (2016) Time-dependent seismic fragility analysis of bridge systems under scour hazard and earthquake loads. Eng. Struct. 121:52-60

Hu S, Chen B, Song G, Wang L (2022) Resilience-based seismic design optimization of highway RC bridges by response surface method and improved non-dominated sorting genetic algorithm. Bull. Earthquake Eng.

Hung C-C, Yau W-G (2017) Vulnerability evaluation of scoured bridges under floods. Engineering Structures 132:288-299

Jabari Salmi Z, Khodakarami MI, Behnamfar F (2024) A Machine Learning-Based Framework for Estimating Fragility Parameters in RC/MR Frames Considering Seismic, Structural, and Site Attributes. Journal of Earthquake Engineering 28(16):4698-4720

Jamdar M, Dolatshahi KM, Yazdanpanah O (2024) Multivariable fragility surfaces for earthquake-induced damage assessment of buildings integrating structural features. Bull. Earthquake Eng. 22(13):6675-6705

Jeon J-S, DesRoches R, Kim T, Choi E (2016) Geometric parameters affecting seismic fragilities of curved multi-frame concrete box-girder bridges with integral abutments. Engineering Structures 122:121-143

Jiao C, Lu Z, Long P, Shi X, Hou S (2018) Study on seismic behavior of curved bridge considering soil-abutment-superstructure interaction. Journal of Vibration and Shock 37(8):99-106

Karriqi T, Matos JC, Dang N-S, Xia Y (2024) Bridge assessment under earthquake and flood-induced scour. Applied Sciences 14(12):5174

Kiani J, Camp C, Pezeshk S (2019) On the application of machine learning techniques to derive seismic fragility curves. Computers & Structures 218:108-122

Li G QP, Dong Z, and Li H (2022) Research Progress on Risk Analysis and Design for Structures under Multiple Hazards of Earthquake and Flood. Journal of Disaster Prevention and Mitigation Engineering 42(02):237-250

Li H, Li L, Wu W, Xu L (2020) Seismic fragility assessment framework for highway bridges based on an improved uniform design-response surface model methodology. Bull. Earthquake Eng. 18(5):2329-2353

Li L, Wu W, Hu S (2024) Theory and Application of Seismic Vulnerability Analysis for Bridge Structures. People's Communications Publishing House Co., Ltd, Beijing

Li Y, Chen H, Yi M, Li J, Fang C (2025) Seismic vulnerability analysis of bridges incorporating scour uncertainty using a copula-based approach. Ocean Eng. 323:120598

Lu G, Wang K, Qiu W, Zhang B (2022) Seismic fragility models of double-column piers of small-and medium-span bridges in highway based on random forest. Earthq. Eng. Eng. Dyn 42:94-103

Medina Yauri DF, Muñoz-Manrique A, Huarca Pulcha A, Espinoza Vigil AJ (2026) An Integrated Resilience Assessment Framework for Riverine Bridges Based on Hydraulic Modeling and Multicriteria Analysis. Water 18(6):746

Nguyen HD, Lee Y-J, LaFave JM, Shin M (2023) Seismic fragility analysis of steel moment frames using machine learning models. Engineering Applications of Artificial Intelligence 126:106976

Ning C, Xie Y, Burton H, Padgett JE (2024) Enabling efficient regional seismic fragility assessment of multi-component bridge portfolios through Gaussian process regression and active learning. Earthquake Engineering & Structural Dynamics 53(9):2929-2949

Nirandjan S, Koks EE, Ye M, Pant R, Van Ginkel KC, Aerts JC, Ward PJ (2024) Physical vulnerability database for critical infrastructure hazard risk assessments–a systematic review and data collection. Natural Hazards and Earth System Sciences 24(12):4341-4368

Padgett JE, Nielson BG, DesRoches R (2008) Selection of optimal intensity measures in probabilistic seismic demand models of highway bridge portfolios. Earthquake Engineering & Structural Dynamics 37(5):711-725

Parisi F, Nettis A, Uva G (2025) Machine learning-aided cloud analysis for seismic fragility assessment of multi-span bridges. Engineering Structures 343:121175

Pinto F, Astroza R, Pizarro A, Bazáez R, Hernández F (2024) Seismic fragility analysis of simply supported bridges considering uncertainty in scour condition. Structures 64:106570

Rashid M, Nishio M (2025) Optimal intensity measure-based seismic fragility surfaces for curved bridges considering their sensitivity to seismic excitation direction. Earthquake Engineering and Engineering Vibration 24(2):509-526

Rezaei H, Zarfam P, Golafshani EM, Amiri GG (2022) Seismic fragility analysis of RC box-girder bridges based on symbolic regression method. Structures 38:306-322

Rezaei H, Zarfam P, Golafshani EM, Amiri GG (2023) Development of seismic demand prediction models for bridges based on probability approach using symbolic regression method. Computers & Structures 282:106991

Ruchun M, Chen L, Xing Z, Ye X, Xiong C, Liu C, Chen Y (2023) Bridge seismic fragility model based on support vector machine and relevance vector machine. Structures 52:768-778

Saida T, Rashid M, Nishio M (2024) System fragility analysis of highway bridge using multi-output Gaussian process regression surrogate model. Advances in Structural Engineering 27(16):2803-2822

Scozzese F, Tubaldi E, Dall'Asta A (2023) Damage metrics for masonry bridges under scour scenarios. Eng. Struct. 296:116914

Serdar N, Folić R (2018) Vulnerability and optimal probabilistic seismic demand model for curved and skewed RC bridges. Engineering Structures 176:411-425

Soleimani F (2022) Probabilistic seismic analysis of bridges through machine learning approaches. Structures 38:157-167

Song S, Xie Y, Wang Y, Zhang W, Kurtulus A, Apaydin NM, Taciroglu E (2024) Seismic fragility and vulnerability assessment of a multi-span irregular curved bridge under spatially varying ground motions. Soil Dynamics and Earthquake Engineering 180:108585

Tehrani P, Heydarpour K (2025) Probabilistic evaluation of combination rules for seismic response prediction of horizontally curved RC bridges under varying earthquake incidence angles. Scientific Reports 15(1):24313

Tian Y, Chen J, Du C, Sun Z, Li Q, Wang D, Wang T (2024) Experimental study on the seismic performance of a curved bridge via large-scale hybrid tests. Engineering Structures 304:117699

Tondini N, Stojadinovic B (2012) Probabilistic seismic demand model for curved reinforced concrete bridges. Bulletin of Earthquake Engineering 10(5):1455-1479

Tubaldi E, Macorini L, Izzuddin BA (2018) Three-dimensional mesoscale modelling of multi-span masonry arch bridges subjected to scour. Engineering Structures 165:486-500

Uenaga T, Omidian P, George RC, Mirzajani M, Khaji N (2023) Seismic resilience assessment of curved reinforced concrete bridge piers through seismic fragility curves considering short-and long-period earthquakes. Sustainability 15(10):7764

Wang D (2024) Research on Machine Learning based Seismic Fragility of Bridges under Random Scouring Action. In: College of Civil Engineering. Xiangtan University, Xiangtan, China

Wang Z, Dueñas-Osorio L, Padgett JE (2014) Influence of scour effects on the seismic response of reinforced concrete bridges. Eng. Struct. 76:202-214

Wu W, Tang S, Hou J, Li H, Elghazouli AY (2025) Seismic performance of continuous rigid-frame bridges affected by flood-induced scour. Structures 71:107944

Wu W, Zhang w, Yao Y, Zhang C (2024) Influence of flood-induced pier and abutment scour on seismic performances for component and entire structure of the reinforced concrete bridges. Journal of Railway Science and Engineering 21(10):4123-4135

Yang J, Ma L (2018) Seismic Response Analysis of Large Span Curved Box Girder Bridge with Small Radius. Highway Engineering 43(01):244-250

Yao Y (2023) Research on Influence of Number for Selected Ground Motions on Seismic Fragility Analysis of the RC Bridge. In: College of Civil Engineering. Xiangtan University, Xiangtan, China

Zheng S, Lei C, H J (2023) Application overview of artificial intelligence technology in bridge seismic field. Earthquake Engineering and Engineering Dynamics 38(07):1-17

Zhong J, Wen J, Wang X (2025) Artificial Intelligence in Bridge Seismic Research:State of the Art and Future Directions. China J. Highw. Transp 38(07):1-17

Authors and Affiliations

Wenpeng Wu[1]

wuwenpeng@xtu.edu.cn

Jiacheng Li[1]

202521652800@smail.xtu.edu.cn

Xin Ye[1,2]

xinye@csu.edu.cn

Jiqiu Zhou[1]

202321652929@smail.xtu.edu.cn

Jiaqing Hou[3]

tony_323@163.com

[1] College of Civil Engineering, Xiangtan University, Xiangtan, China

[2] School of Civil Engineering, Central South University, Changsha, China

[3] PowerChina Zhongnan Engineering Co. Ltd, Changsha, , China